

The University of North Carolina
at Greensboro

JACKSON LIBRARY



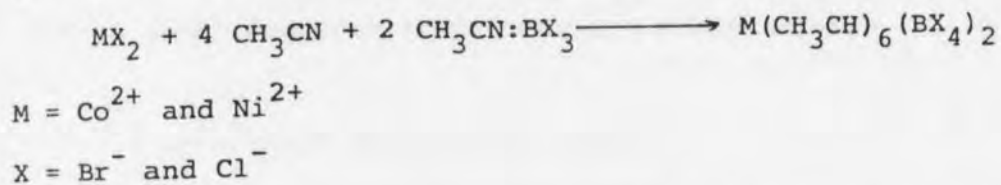
CQ

no. 1641

UNIVERSITY ARCHIVES

KONG, PETER CHUEN SUN. An Experimental and Theoretical Study of Cobalt(II) and Nickel(II) Complexes with Acetonitrile as Ligand. (1978)
Directed by: Drs. Joseph A. Dilts and John L. Graves.
Pp. 78

Cobalt(II) and nickel(II) halides form complexes with acetonitrile as ligands and boron trihalides as counter ions. The reaction is represented by the general equation:



The reaction mechanism involves halide ion transfer from the transition metal halides to the boron trihalides, forming the tetrahaloborate species. The ligand-field model is a trigonally distorted octahedron. All the complexes are air sensitive and air-free synthetic techniques are required.

Elemental analysis and X-ray studies are used to obtain molecular geometry and configurational information about the molecule. Thermal analyses and kinetics studies are applied to compare the relative strength of the bonds between nickel and cobalt complexes. The activation energy and the order of reaction is estimated for the thermal decomposition reaction. IR spectra reveal a positive shift in the nitrile frequency when acetonitrile is coordinated to metal ions. Ligand-field spectra are utilized to explain the structures of the acetonitrile solvated nickel(II) and cobalt(II) cations.

Dedication

I dedicate this thesis and the poem to my deceased father and the surviving members of my family to whom I owe a great deal for their love and expectations.

I am a small humble sand pebble,
Lying lazily on the water front,
Wetting myself with the spray from the oncoming tides,
Waiting for that one big wave which will carry me to
the ocean
To probe its depths.

Knowledge is what I am hungering for,
Ability to see the beauty within.
It is the ultimate reward.

Peter C. Kong

JNU C. LIBRARY

AN EXPERIMENTAL AND THEORETICAL STUDY OF
COBALT(II) AND NICKEL(II) COMPLEXES
WITH ACETONITRILE AS LIGANDS

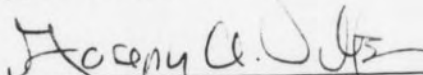
by

PETER CHUEN SUN KONG

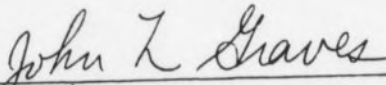
A Thesis Submitted to
the Faculty of the Graduate School at
The University of North Carolina at Greensboro
in Partial Fulfillment
of the Requirements for the Degree
Master of Science

Greensboro
1978

Approved by



Thesis Advisor



Thesis Advisor

UNIVERSITY OF NORTH CAROLINA LIBRARY

28112

APPROVAL PAGE

This thesis has been approved by the following committee of the Faculty of the Graduate School at the University of North Carolina at Greensboro.

Thesis Advisors

Joseph C. Olt

John L Graves

Committee Members

Walter N. Pitts

John L Graves

T.A. Nile

Joseph C. Olt

April 14, 1978

Date of Oral Examination

ACKNOWLEDGEMENTS

I would like to thank Drs. Joseph A. Dilts and John L. Graves for their professional assistance, guidance, patience and encouragement in the preparation of this thesis. I am grateful to the Graduate School of the University of North Carolina at Greensboro for the generous financial support during this course of study. The author would like to express his gratitude to the members of the faculty and staff of the Chemistry Department for their instruction, constructive criticisms, friendship and recommendations during his period of residence. Thanks to Mr. Stephen Adams for the illustrations herein, and Mrs. Betsy Mosteller for typing the thesis.

UNC LIBRARY

TABLE OF CONTENTS

	Page
Approval Page	ii
Acknowledgements	iii
List of Tables	v
List of Figures	vi
Statement of Problem	vii
Chapter 1 INTRODUCTION	1
Chapter 2 THEORETICAL TREATMENT	10
The Crystal Field Potential	13
Chapter 3 EXPERIMENTAL PROCEDURES	27
Preparation of Anhydrous Nickel(II) Chloride	27
Preparation of Anhydrous Cobalt(II) Chloride	28
Preparation of Anhydrous Nickel(II) Bromide	29
Preparation of Anhydrous Cobalt(II) Bromide	30
Preparation of Acetonitrile Boron Trihalides Adducts	31
Synthesis of Transition Metal Complexes	35
Thermal Analyses Procedures	39
X-ray Analyses Procedures	41
Infrared Analyses Procedures	41
Ligand-field Analyses Procedures	41
Chapter 4 RESULTS AND DISCUSSIONS	42
Elemental Analyses	42
Thermal Decomposition Analyses	45
X-ray Powder Analyses	50
Infrared Analyses	53
Ligand-field Analyses	54
Summary	56
Bibliography	64
Appendix I	67

LIST OF TABLES

	Page
TABLE 1. The Correlation Table Between Point Group O_h and D_{3d}	18
TABLE 2. The Recursion Relations for the Reducible Representations of the Point Group O_h	18
TABLE 3. The Reducible Representations for the Free Ion States in Octahedral Point Group	19
TABLE 4. The Reducible Representations for the Free Ion States in D_{3d} Point Group	19
TABLE 5. Values of the Angles of this D_{3d} Model	21
TABLE 6. Comparison of the Spin-orbit Coupling Constants with Ground State Transitions and the Ligand-field Parameters Dq and B	24
TABLE 7a. Spherical Harmonics of Order 6 in Spherical Polar Coordinations	25
TABLE 7b. Spherical Harmonics of Order 6 in Cartesian Coordinates	26
TABLE 8. Elemental Analysis of the Percentage of C, H, N and B in the Complexes	43
TABLE 9. Theoretical Calculated Elemental Analysis of C, H, N and B in the Complexes	43
Table 10. Theoretical Calculated Values of the Percentages of C, H, N and B in the Complexes with the Inclusion of $B(OH)_3$	44
TABLE 11. Comparison Between DSC and DTG Data	48
TABLE 12. TG/DTG Data of the Complexes $Ni(CH_3CH)_6 \cdot (BCl_4)_2$ and $Co(CH_3CN)_6(BCl_4)_2$	49
TABLE 13. X-ray Powder Diffraction Patterns for the Compounds	52
TABLE 14. Comparison of the IR Frequency Shifts Between the Free Ligands and the Complexes	53

LIST OF FIGURES

	Page
FIG. 1. The Point Charge for the D_{3d} Model	20
FIG. 2. Definition of Axes	20
FIG. 3. Splittings of the T_{2g} Orbitals under Trigonal Distortion. Symmetry Lowering from O_h to D_{3d} .	22
FIG. 4. Apparatus for the Synthesis of Complexes	58
FIG. 5. Extraction of the Complex from Impurities	59
FIG. 6. TG/DTG Curves of $Ni(CH_3CN)_6(BCl_4)_2$	60
FIG. 7. DSC Curve of $Ni(CH_3CN)_6(BCl_4)_2$	61
FIG. 8. DSC Curve of $Co(CH_3CN)_6(BCl_4)_2$	62
FIG. 9. TG/DTG Curves of $Co(CH_3CN)_6(BCl_4)_2$	63

STATEMENT OF PROBLEM

Acetonitrile is a weak base and is not frequently used as a ligand in coordination chemistry investigations. Due to the nature of this ligand, it was thought that cobalt(II) and nickel(II) complexes with acetonitrile ligands would be unstable and that the solid state of these complexes probably would not exist.

Basolo¹ indicated that solid salts separated from solution easiest for combinations of either small-small or large-large cations and anions, preferably with systems having the same but opposite charges on the counter ions. The driving force for the large cation-large anion combination to form solid is the small hydration energy of the ions. When Co(II) and Ni(II) are completely solvated by acetonitrile, they form large cations; these large cations could be effectively stabilized by large anions such as tetrachlorometallates or tetrabromometallates. The purpose of this study is fourfold. The first is to synthesize the complexes by using large anions, BCl_4^- and BBr_4^- . The second is to compare results with similar systems. The third is to make theoretical investigations of the molecular model assuming distortion and the last is to analyze the complexes experimentally.

CHAPTER 1

INTRODUCTION

A number of the complex compounds of the general formula $M(\text{CH}_3\text{CN})_n^{\text{P}+} (\text{M}'\text{X}_4^-)_p^{1a}$ and $M(\text{R}_2\text{-S=O})_6 (\text{A})_n^2$ have been reported over the decade of 1960 to 1970. In these complexes the cations are the divalent metals (Mg(II), Ca(II), Mn(II), Fe(II), Co(II), Ni(II), Cu(II) and Zn(II)) and the anions are tetrachlorometallates¹ (BCl_4^- , AlCl_4^- , InCl_4^- and FeCl_4^-) or tetrabromometallates³ (AlBr_4^- , GaBr_4^- , InBr_4^- and FeBr_4^-). The ligands of the complexes $M(\text{R}_2\text{S=O})_6 (\text{A})_n$ are

DTMSO (1,4-dithiane monosulfoxide, $\text{S} \begin{array}{l} \text{CH}_2-\text{CH}_2 \\ \text{CH}_2-\text{CH}_2 \end{array} \text{S=O})^4$, DMSO (dimethyl sulfoxide, $\text{H}_3\text{C}-\overset{\text{O}}{\parallel}{\text{S}}-\text{CH}_3$)^{4,5}, PMSO (pentamethylene sulfoxide, $\text{CH}_2 \begin{array}{l} \text{CH}_2-\text{CH}_2 \\ \text{CH}_2-\text{CH}_2 \end{array} \overset{\text{O}}{\parallel}{\text{S}}=\text{O})^4,6,7$, TOSO (1,4-thioxane sulfoxide, $\text{O} \begin{array}{l} \text{CH}_2-\text{CH}_2 \\ \text{CH}_2-\text{CH}_2 \end{array} \text{S=O})^4$, DPSO (diphenyl sulfoxide, $\text{O} \begin{array}{l} \text{CH}_2-\text{CH}_2 \\ \text{CH}_2-\text{CH}_2 \end{array} \overset{\text{O}}{\parallel}{\text{S}}-\text{O})^8,9$ and MPSO (methyl phenyl sulfoxide, $\text{H}_3\text{C}-\overset{\text{O}}{\parallel}{\text{S}}-\text{O})^{10}$.

The anions of these complexes are BF_4^- and ClO_4^- . These sulfoxides constitute an interesting class of ligands. Both the sulfoxide group and the sulfide atom in the DTMSO molecule can donate a lone pair of electrons to the metal cations, M^{2+} . The oxide atom or the sulfoxide group in the TOSO molecule can donate a lone pair of electrons to the metal cations for bonding.

The infrared vibrational spectra¹¹ and the UV-visible ligand field spectra¹² of these complexes indicate the bonding is via the sulfoxide group and not via the sulfur atom in DTMSO or the oxygen atom in TOSO ligands. In all other metal complexes containing DMSO, DPSO, MPSO and PMSO as ligands, the bonding is through the sulfoxide group. The crystal field splitting parameters¹² (Dq values) of both Co(II) and Ni(II) with TOSO, PMSO and DTMSO as ligands have been compared. The Dq values follow the same pattern regardless of the metal cations. The spectrochemical series of these ligands is PMSO>TOSO>DTMSO. In these complexes only the atoms placed para to the sulfoxide group are varies. The Dq values for these ligands with respect to the same metal ion may be attributed to the differences in electronegativities of the ligands. The metals have no effect on the Dq values since both nickel and cobalt have essentially the same electronegativity, but the influence of the effective nuclear charge on the metal ions bears some importance. Between the two, Ni(II) has a higher Z_{eff} thus a lower Dq value than Co(II) indicating a more stable complex formation. This possibly accounts for the positions of the ligands in the spectrochemical series and the comparison between nickel and cobalt ions with the same ligand. A closer look at the complexes of Ni(II) and Co(II) with TOSO, PMSO and DTMSO as ligands, shows the variation of Dq values for these

ligands with respect to the differences in the electronegativities of the substituents on the ligand and probably more so on the number of lone pairs of electrons on the substituted atom.

Among all the sulfoxide ligands studied by Reedijk et al⁴, the most interesting ligand was DTMSO since both the sulfide, (S-atom) and the sulfoxide group, (S=O) can donate their lone pair of electrons to the metal ion for bonding. Their infrared studies indicated that the complex bonding is via the sulfoxide group and not the sulfide group. The sulfoxide group stretches appear in the region below 960 cm^{-1} in the infrared spectra. The band shapes are rather sharp and without splittings which fact indicates that all the six ligands are coordinated in the same way and probably are arranged in a fairly regular octahedron. The S=O stretches for the free ligands appear in the region of $1045\text{--}1064\text{ cm}^{-1}$ and this shift to lower frequency has been interpreted in terms of oxygen coordination of the S=O link towards the metal ions. The magnitude of the shift can be taken as a rough measure of the electronegativity of the metal ions. Similar shifts of the same order of magnitude were also observed for other sulfoxide ligands. The occurrence of the metal-ligand pure stretching vibrations has not been observed and this is probably due to its interaction with the internal vibration of the ligands. A shift to longer wavelengths in the S=O stretching frequencies upon coordination with the metal ions was also observed in complexes containing

ligands with carbonyl (C=O) functional groups¹³ and with phosphine oxide (P=O) functional groups¹⁴. These observations were interpretable in terms of a decrease of the force constants of the C=O, P=O and S=O bonds respectively.

In the complexes with ligands containing nitrile groups, the opposite effect has been observed. The shift in C≡N stretching frequencies upon coordination with metal ions is to shorter wavelength. This is interpreted in terms of an increase in the force constant of the C≡N stretching vibrations, that is the bond energy in the nitrile group increases. The coordination of the ligands is via the lone pair of electrons on the nitrogen atom, and all the ligands should coordinate in the same manner.

Recently Purcell¹⁵ stated that all nitriles and isonitriles coordinated to metal ions show an increased C≡N force constant due to the strengthening of the sigma (δ) bonding between the carbon and the nitrogen atoms. In addition to this δ character, the nitrogen lone pair orbital will acquire some pi (π) character upon coordination to the metal ion, which means that an increasing amount of δ character in the sigma bond of the nitrile resulting in an increasing force constant.

Reedijk et al¹⁶ made an extensive investigation on the infrared spectra of coordinated methyl cyanide with different metal ions. They compared the frequency shifts of all eight normal modes of vibrations in the coordinated acetonitrile

with the standard noncoordinated acetonitrile. Particularly when comparing with the frequency shifts of CH_3CN coordinated to Co(II) and Ni(II) cations, the shift to higher frequencies in $\text{Ni}(\text{CH}_3\text{CN})_6^{2+}$ vs $\text{Co}(\text{CH}_3\text{CN})_6^{2+}$ indicate that the bonding in the nickel complex is stronger than that of cobalt. Their results are consistent with the observation obtained in the sulfoxide ligand investigations. Based on the evidence of increasing pi character in the nitrogen lone pair and the increasing sigma character in the CN bond upon coordination of the acetonitrile to metal ions, two factors seem to be important in explaining this frequency increase:

- (1) Kinematic Coupling of CN and Metal-nitrogen Stretching Vibrations.

For the linear system Me-CN:M^{2+} , the lone pair of electrons on nitrogen due to the bonding with M^{2+} acquires some pi character. Then the coupling of CN and N:M^{2+} stretching vibration should give rise to a small increase in the CN stretching frequency. The electron density shifts from the nitrogen atom to offset the electron density shifts from the nitrogen lone pair to the metal cation. That is the metal ion withdraws the electron density from the nitrogen atom. This results in the small increase in the CN bond strength. The explanation is consistent with the valence-field calculation demonstration by Brown and Kubota¹⁷.

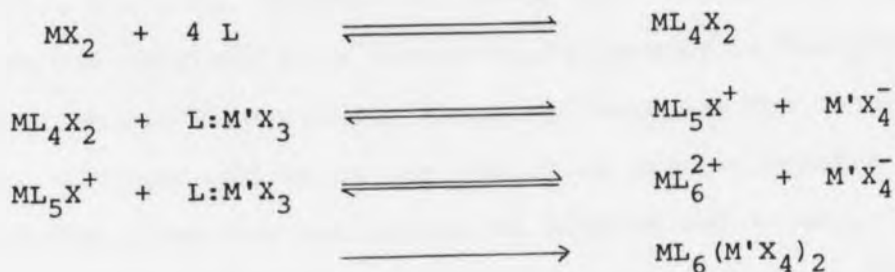
(2) Ionic Contribution to the CN Bond.

The force constant of the CH or CN covalent bond depends to a large extent on the polar character of the bond. A small percentage increase in the ionic character of the bond would increase the force constant, whereas a large increase would decrease it. The force constant is related to the bond length and to the bond dissociation energy. When the ionic character in a bond increases slightly, the stronger electrostatic attraction will cause the bond length to shrink. Thus a shorter bond length increases the force constant. But when there is a large increase in ionic character, repulsive forces from the nuclei and the subshell electrons of both atoms involved in the bonding are strong which tends to decrease the bond dissociation energy and increase the internuclear distance. As a result the force constant decreases. A shifting of the electron density in the CN bond would result in an increase in the δ character of the bond. The small increment in the polar nature of the CN bond may well give a shorter and stronger bond. This would increase the force constant on the CN bond upon coordination with metal ions.

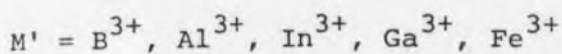
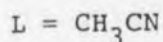
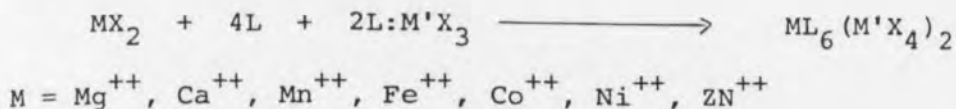
The strength of CN bonds depends critically on the percentage of ionic character and this in turn determines the direction of the frequency shift. Although kinematic coupling

and increase in ionic character of the CN bond contribute to the frequency increase, neither is solely responsible for this. There are other influences on the CN frequency shift which are less well understood at present.

The first compounds with acetonitrile solvated cations were reported by Zuur¹⁸. The anions for these complexes were tetrachlorometallates and tetrabromometallates. These cations are completely solvated in acetonitrile. Early workers had attempted unsuccessfully to make this class of compounds. The main difficulty was to remove all the water from the hydrated cation and to replace them with acetonitrile molecules. The compounds were synthesized in acetonitrile by reaction of the metal chlorides with group III A metal chlorides and FeCl_3 . The tetrabromometallates were prepared by a similar reaction. The reaction mechanism involves chloride or bromide ion transfer from the divalent metal chloride/bromide to the metal trichlorides forming the tetrahalometallate species. Reaction scheme:



The overall reaction is given below:



X-ray powder analysis indicated a large number of these complexes are isomorphous.

Reedijk^{1a} grouped these complexes according to the X-ray diffraction patterns. He found that the crystal type formed was characteristic of each diffraction pattern. The X-ray pattern of the class (labeled C) to which $Co(CH_3CN)_6(BCl_4)_2$ and $Ni(CH_3CN)_6(BCl_4)_2$ belonged formed hexagonal plates after recrystallization. In our work hexagonal crystals were observed in freshly prepared samples of all the complexes except $Ni(CH_3CN)_6(BCl_4)_2$. In diffraction patterns made later of each complex, all except $Co(CH_3CN)_6(BBr_4)_2$ had similar diffraction pattern. Information about the structure of the complexes was obtained from ligand-field spectra in the present work and from the literature. Elemental analyses for carbon, hydrogen, nitrogen and boron were obtained from an outside laboratory to check for the number of ligands and anions. Thermal analysis experiments were carried out to compare the bond strength between the metal ions and ligands. This

information can be used to compare the relative electronegativities of the metal ions.

Until now there have been no reports on the other two complexes, $\text{Ni}(\text{CH}_3\text{CN})_6(\text{BBr}_4)_2$ and $\text{Co}(\text{CH}_3\text{CN})_6(\text{BBr}_4)_2$. There is no reason to believe these two complexes would behave differently from the other two of the series. Previous workers indicated that the structures of $\text{Ni}(\text{CH}_3\text{CN})_6(\text{BCl}_4)_2$ and $\text{Co}(\text{CH}_3\text{CN})_6(\text{BCl}_4)_2$ involve a regular octahedral species. These ligand-field spectra were recorded at room temperatures and there was a problem with degeneracies. To remove degeneracy low temperature must be used to study the features in ligand-field spectra. A true structure cannot be determined without the aid of low temperature ligand-field spectra. In solution, because of the dissociation of the ion pairs, we can assume the cationic species to be octahedral. But in the crystalline state, due to the incorporation of the anions in the rigid lattice, the geometric structure could be deformed to a lower symmetry. By looking at a molecular model, a trigonal distortion of the regular octahedron seems possible. Assuming trigonal distortions we can look into the ligand-field potential for this system.

CHAPTER 2THEORETICAL TREATMENT

In acetonitrile there is a lone pair of electrons on the nitrogen atom. Due to electrostatic interaction with the cobalt or nickel nuclei, the electron pair in the ligand is directed towards the metal to form the complexed cation, ML_6^{++} . The ligands are arranged themselves along the intercoordination axes to form an octahedron, either regular or distorted. In the solution phase the ions dissociate and the octahedron is regular. In the solid phase, when the cation and the anion are combined to form a stable crystalline structure, then the perfect octahedron of the cation may be distorted to achieve close packing with the anion. If the distortion is either compression or elongation along one of the body diagonal axes, the O_h symmetry will be destroyed. The symmetry of the molecule would be lowered from O_h to D_{3d} , as a result of trigonal distortion. The crystal field potential is expressed as a combination of the trigonal and the octahedral potentials. The potential is written as a product of the radial and the angular part of the d orbital wave functions. The angular part of the wave function is expressed in terms of the spherical harmonics. The quantum mechanical treatment of the crystal field model is easily formulated^{19,20}. The Hamiltonian for

the metal ion electrons consists of two terms:

$$H = H_f + V_L$$

H_f is the Hamiltonian for the free ion and V_L is the ligand field potential. V_L is regarded as the perturbation for the system which influences the electronic motions and the term values of the metal ion in the complex. The Hamiltonian²¹ for the free ion is given as:

$$H_f = -\frac{\hbar^2}{2m} \sum_i \nabla_i^2 - \sum_i \frac{Ze^2}{r_i} + \frac{1}{2} \sum_{j \neq i} \frac{e^2}{r_{ij}} + \sum_i \xi_i(r) \vec{L}_i \cdot \vec{S}_i$$

The first two terms are the Hamiltonian one electron operator, the third term is the pair-wise electronic interactions and the fourth term is the spin-orbit interactions of the free ion. Since the system is going to be perturbed by V_L , it is important to know how V_L compares in order of magnitude with these two perturbing quantities.

When a transition metal ion is placed in a crystal potential, the energy level of the free ionic states are split into crystal levels. One assumption made is that the crystal splitting is smaller than the energy separations associated with the principal and azimuthal quantum numbers (n, l) and these quantum numbers are good to the first approximation in the crystal potential. The first approximation²² assumes that the radius of the free ion in its ground state and the lower excited state is the same. The comparison of

the relative magnitudes of these perturbing quantities can be generalized into three cases²³:

(A) The Very Weak Field Approximation

$$\xi(r) \vec{L} \cdot \vec{s} > V_L(r)$$

The energy separation arising from spin-orbit interactions is larger than the crystal field splitting due to the ligand field potential. These are mostly observed in the rare-earth group ions in crystals.

(B) The Weak Field Approximation

$$\frac{e^2}{r_{ij}} > V_L(r) > \xi(r) \vec{L} \cdot \vec{s}$$

The crystal field separation due to the ligand field potential is smaller than the pair-wise electronic interactions, which can be calculated within the Russell-Saunders terms ^{2S+1}L , but it is larger than the energy level splitting arising from the spin-orbit interactions. These are mostly observed in the complexes of the first transition groups.

(C) The Strong Field Approximation

$$V_L(r) > \frac{e^2}{r_{ij}}$$

The crystal field separation due to the ligand field potential is larger than the separation arising from the electronic interaction. These are observed in the covalent

complexes.

This classification of field strength is only approximate, yet it is convenient for calculating the crystal field effect.

The Crystal Field Potential

The single ion model treats the ligands which surround the transition metal ion as a cavity. This cavity provides a constant electrostatic field for the metal ion electrons when the ion is placed in the center of this cavity. The metal ion electrons will be subjected to the influence of this spherical electric field produced by the ligands. This field maintains a constant effective potential in the cavity, in which the electrons of the metal ion move. Based on electrostatic theory, this effective potential in the cavity must satisfy Poisson's equation²⁴:

$$\vec{\nabla} \cdot \vec{E}_L(r) = 4\pi\rho_L(r)$$

$$\vec{E}_L(r) = -\vec{\nabla} V_L(r)$$

$$\nabla^2 V_L(r) = -4\pi\rho_L(r)$$

\vec{E}_L = electric field associated with the ligands

ρ_L = charge density of the ligands

V_L = effective ligand potential

Outside the cavity, the region of space has no charge density, $\rho_L(r) = 0$; then the equation becomes the Laplace equation:

$$\nabla^2 V_L(r) = 0$$

The potential is most conveniently expressed in terms of the radial and the spherical harmonics basis functions²⁵.

$$V_L(r, \theta, \phi) = \sum_{n=0}^{\infty} \sum_{m=n}^{-n} A_n^m \cdot r^n \cdot Y_n^m(\theta, \phi)$$

A_n^m is the expansion coefficients of the potential with respect to the basis functions r^n and $Y_n^m(\theta, \phi)$. r^n is the radial basis function and $Y_n^m(\theta, \phi)$ is the spherical harmonics basis function, and n is the order of the function. Upon expansion, V_L takes the form:

$$V_L = A_0^0 r^0 Y_0^0 + A_1^1 r^1 Y_1^1 + A_1^0 r^1 Y_1^0 + A_1^{-1} r^1 Y_1^{-1} + \dots$$

Since we are only dealing with the metal d orbitals, Y_n^m of order higher than four will vanish²⁶. Using the point charge model^{27,28}, the expansion coefficients are found to be:

$$A_n^m = \frac{4\pi}{2n+1} (-1)^m \sum_j e_j \cdot r_j^{-(n+1)} \cdot Y_n^{-m}(\theta, \phi)$$

where j is summed over all the point charges on the lattice sites. The spherical harmonics (Y_n^m and Y_n^{-m})²⁹ are given below:

$$Y_n^m(\theta, \phi) = (-1)^m \left(\frac{2n+1}{4\pi}\right)^{1/2} \left(\frac{(n-m)!}{(n-m)!}\right)^{1/2} P_n^m(\cos \theta) e^{im\phi}$$

$$\text{and } Y_n^{-m}(\theta, \phi) = \left(\frac{2n+1}{4\pi}\right)^{1/2} \left(\frac{(n-m)!}{(n-m)!}\right)^{1/2} P_n^m(\cos \theta) e^{im\phi}$$

$(-1)^m$ is called the Condon and Shortley phase³⁰. $P_n^m(\cos \theta)$

is the associated Legendre Polynomial of degree n . The

effect of this phase is to introduce an alternation of sign among the positive m spherical harmonics. The spherical harmonics, Y_n^m and Y_n^{-m} and the expansion coefficients A_n^m and A_n^{-m} are proportional to each other.

$$Y_n^m = (-1)^m K e^{im\theta}$$

$$(Y_n^m)^* = (-1)^m K e^{-im\theta}$$

$$(-1)^m (Y_n^m)^* = K e^{im\theta}$$

$$(-1)^m (Y_n^m)^* = Y_n^{-m}$$

K = the normalization constants and polynomial in θ .

Similarly:

$$(-1)^m (Y_n^{-m})^* = Y_n^m$$

Also

$$A_n^m = \frac{4\pi(-1)^m}{2n+1} \sum_j e_j r_j^{-(n+1)} (Y_n^{-m}(\theta, \theta))$$

$$(A_n^m)^* = \frac{4\pi}{2n+1} (-1)^m \sum_j e_j r_j^{-(n+1)} (Y_n^{-m}(\theta, \theta))^*$$

$$(-1)^m (A_n^m)^* = \frac{4\pi}{2n+1} (-1)^m \sum_j e_j r_j^{-(n+1)} (-1)^m (Y_n^{-m}(\theta, \theta))^*$$

$$= \frac{4\pi}{2n+1} (-1)^m \sum_j e_j r_j^{-(n+1)} Y_n^m(\theta, \theta)$$

$$= A_n^{-m}$$

and

$$(-1)^m (A_n^{-m})^* = A_n^m$$

Since the electrostatic potential must be real, the spherical harmonics and the expansion coefficients must transform into each other accordingly.

$$Y_n^{-m}(\theta, \varphi) = (-1)^m (Y_n^m(\theta, \varphi))^* ; A_n^{-m} = (-1)^m (A_n^m)^*$$

$$Y_n^m(\theta, \varphi) = (-1)^m (Y_n^{-m}(\theta, \varphi))^* ; A_n^m = (-1)^m (A_n^{-m})^*$$

It is easily seen that $(-1)^m Y_n^{-m}(\theta, \varphi) = (Y_n^m(\theta, \varphi))^*$ then A_n^m takes the form

$$A_n^m = \frac{4\pi}{2n+1} \sum_j e_j r_j^{-(n+1)} (Y_n^m(\theta_j, \varphi_j))^*$$

Substituting A_n^m into the expression for V_L , we get

$$\begin{aligned} V_L(r, \theta, \varphi) &= \sum_{n=0}^{\infty} \sum_{m=-n}^{-n} \frac{4\pi}{2n+1} \sum_j e_j \frac{r^n}{r_j^{n+1}} (Y_n^m(\theta_j, \varphi_j))^* Y_n^m(\theta, \varphi) \quad (I) \\ &= \sum_j \frac{r_j}{|\vec{r} - \vec{r}_j|} \end{aligned}$$

which is the multipole expansion³¹ of the point charges

potential. The radial term, $\frac{r^n}{r_j^{n+1}}$, in the final effective expression is the radial basis function of the d orbital wave function in our system of interest. Tables of the spherical harmonics in spherical polar coordinates and in Cartesian coordinates are given at the end of this chapter.

The Crystal Field Potential for D_{3d} Symmetry Point Group

If an octahedron is distorted along the threefold axis or the body diagonal of a cube, which bounds the vertices of

a regular octahedron, it is called trigonal distortion. This trigonal distortion results in a lowering of the molecular symmetry from O_h point group to D_{3d} point group. The crystal field potential produced by the ligands is no longer octahedral. The transition metal d electrons also experience another field component which contributes to the total field due to the trigonal distortion. This component is regarded as the trigonal field. The total field produced by the ligands then take the form:

$$V_{L(D_{3d})}(r, \theta, \phi) = V_{O_h}(r, \theta, \phi) + V_t(r, \theta, \phi)$$

If it is seen that there is a correlation between the points O_h and D_{3d} . We can look at the classes of the elements which are common to both point groups. From the character tables of O_h and D_{3d} , we can clearly see that the irreducible representations A_{1g} , A_{2g} , E_g and A_{1u} , A_{2u} , E_u are identical for both point groups. Whereas the irreducible representations T_{1g} , T_{2g} , T_{1u} , T_{2u} in point group O_h are represented by $A_{2g} + E_g$, $A_{1g} + E_g$, $A_{2u} + E_u$ and $A_{1u} + E_u$. Since the u and g terms are correlated with each other in both point groups, we can drop the subscripts u and g. This gives us the general correlation relations between the two point groups.

O_h	D_{3d}
A_1	A_1
A_2	A_2
E	E
T_1	$A_2 + E$
T_2	$A_1 + E$

Table 1³². The correlation table between point groups O_h and D_{3d} .

The reducible representation of the free ion states for D_{3d} can be easily deduced from the correlation table just listed above. Either using $\frac{\sin(L+1/2)\theta}{\sin(\theta/2)}$ ³³ or the recursion table (Table 2) I derived for the octahedral point group, the free ion states for d^n electrons can be generated. In the recursion table, k is a positive integer.

	E	C_3	C_2	C_2	C_4
		1 $L=3k$			1 $L=4k, 4k+1$
$\Gamma_r^{L_i}$	$2L_i+1$	0 $L=3k+1$	$(-1)^{L_i}$	$(-1)^{L_i}$	
		-1 $L=3k+2$			-1 $L=4k+2, 4k+3$

Table 2. The recursion relations for the reducible representations of point group O_h .

The reducible representation is a direct sum of the irreducible representations. For the octahedral point group, we have

Γ_r	L	$\Gamma_{ir}(O_h)$
S	0	A_1
P	1	T_1
D	2	$E + T_2$
F	3	$A_2 + T_1 + T_2$
G	4	$A_1 + E + T_1 + T_2$
H	5	$E + 2T_1 + T_2$

Table 3³⁴. The reducible representations for the free ion states in octahedral point group.

Using Table 1, the reducible representations of the free ion states of the point group D_{3d} are found to be

Γ_r	L	$\Gamma_{ir}(D_{3d})$
S	0	A_1
P	1	$A_2 + E$
D	2	$A_1 + 2E$
F	3	$A_1 + 2A_2 + 2E$
G	4	$2A_1 + A_2 + 3E$
H	5	$A_1 + 2A_2 + 4E$

Table 4. The reducible representations for the free ion states in D_{3d} point group.

If we take the wave functions and quantize along the threefold axis, we get the octahedral field and the trigonal field³⁵ as:

$$V_{O_h}(\theta, \varphi) = b' Y_4^0(\theta, \varphi) + c(Y_4^3(\theta, \varphi) - Y_4^{-3}(\theta, \varphi))$$

and

$$V_t(\theta, \varphi) = a Y_2^0(\theta, \varphi) + b'' Y_4^0(\theta, \varphi)$$

combining these two potentials we get

$$V_{L(D_{3d})}(\theta, \varphi) = a Y_2^0(\theta, \varphi) + b Y_4^0(\theta, \varphi) + c(Y_4^3(\theta, \varphi) - Y_4^{-3}(\theta, \varphi))$$

where a , b , c are independent parameters which include the radial basis functions, the effective charges and the normalization factors. If we look at the molecular geometry of D_{3d} point group below, we can find a complete expression for the potential.

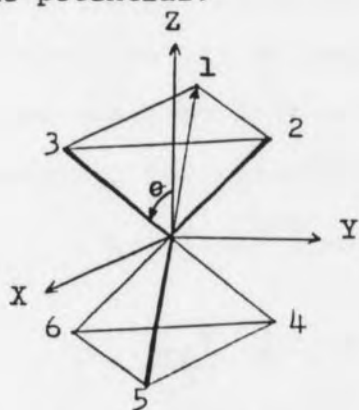


Fig. 1 The point charges for the D_{3d} model.

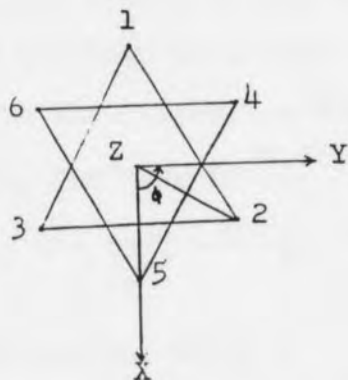


Fig. 2. Definition of axes.

Point	θ	ϕ
1	θ	π
2	θ	$\pi/3$
3	θ	$-\pi/3$
4	$\pi-\theta$	$2\pi/3$
5	$\pi-\theta$	0
6	$\pi-\theta$	$-2\pi/3$

Table 5. Values of the angles of this D_{3d} model.

θ measures from the positive z-axis.

ϕ measures from the positive x-axis through the positive y-axis.

The chokes axis rotates in a right hand screw sense.

Expanding the potential in harmonics and center on the metal, we use equation (I) on page 16 for d orbitals with bond distances equal to R from the metal to the ligand, we have the potential for molecules having D_{3d} symmetry as^{36,37}:

$$V_{L(D_{3d})} = 6 \left(\frac{\pi}{5} \right)^{1/2} \frac{ze r^2}{R^3} (3 \cos^2 \theta - 1) Y_2^0 + \left(\frac{\pi}{2} \right)^{1/2} \frac{ze r^4}{R^5} \times (35 \cos^4 \theta - 30 \cos^2 \theta + 3) Y_4^0 + (35 \pi)^{1/2} \times (\sin^3 \theta) (Y_4^3 - Y_4^{-3})$$

ze is the total charge on the metal ion and r is the average radius of the metal d electron from the nucleus.

The d orbitals of a transition metal ion are split into a group of triply degenerate T_{2g} orbitals and a set of doubly degenerate E_g orbitals when they are placed in an octahedral field. The T_{2g} orbital degeneracy is being removed by the lowering of the molecular symmetry from O_h to D_{3d} due to the trigonal distortion. The T_{2g} orbitals are split into a singly and a double degenerate A_{1g} and E_g orbitals. Whereas the E_g orbitals remain double degenerate.

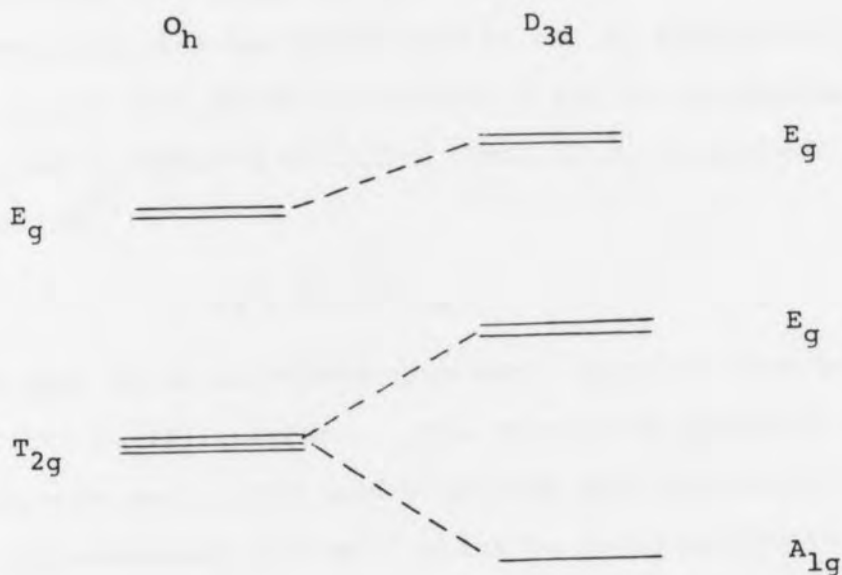


Fig. 3³⁶. Splittings of the T_{2g} orbitals under trigonal distortion. Symmetry lowering from O_h to D_{3d} .

In the D_{3d} point group, the crystal field terms transform as E_g (from E_g in O_h), and E_g and A_{1g} (from T_{2g} in O_h). The two E_g terms can mix by the crystal field operator, that

is the excited state terms can affect the ground state terms by the trigonal field and by spin-orbit coupling.

In weak field approximations, the crystal field term, V_L , is larger than the spin-orbit coupling, $\xi \times L \cdot s$. ξ is the one electron parameter which incorporates the spin-orbit coupling constant λ . There exists a simple relationship between the parameters λ , B and Dq . B is called the Racah parameter, a measure for the interelectronic repulsion which associates with the third term in the H_F expression on page 11. Dq is the well known crystal-field energy separation between t_{2g} and e_g metal d orbitals. Reedijk et al derived the equation³⁸:

$$-\lambda = 0.27B^2/Dq$$

and used it to calculate spin-orbit coupling constants for several Ni(II) complexes. The calculated coupling constants were very small; the band width for the spin-orbit coupling is approximately 100 cm^{-1} , which is about one-tenth of the observed band width for the other transitions. These fine structures cannot be observed at room temperature due to the temperature broadening of the bands. These table below compares all the transitions of $\text{Ni}(\text{CH}_3\text{CN})_6^{2+}$ and $\text{Co}(\text{CH}_3\text{CN})_6^{2+}$ with the calculated spin-orbit coupling constants. The electronic transitions were measured at room temperature by Reedijk⁵⁸.

Table 7a³⁹. Spherical Harmonics of order 6 in spherical polar coordinates.

$$\begin{aligned}
 Y_{00} &= \left(\frac{1}{4\pi}\right)^{1/2} \\
 Y_{10} &= \left(\frac{3}{4\pi}\right)^{1/2} \cos \theta \\
 Y_{1\pm 1} &= \mp \left(\frac{3}{4\pi}\right)^{1/2} \left(\frac{1}{2}\right)^{1/2} \sin \theta e^{\pm i\phi} \\
 Y_{20} &= \left(\frac{5}{4\pi}\right)^{1/2} \frac{1}{2} (3 \cos^2 \theta - 1) \\
 Y_{2\pm 1} &= \mp \left(\frac{5}{4\pi}\right)^{1/2} \left(\frac{3}{2}\right)^{1/2} \sin \theta \cos \theta e^{\pm i\phi} \\
 Y_{2\pm 2} &= \left(\frac{5}{4\pi}\right)^{1/2} \left(\frac{3}{8}\right)^{1/2} \sin^2 \theta e^{\pm 2i\phi} \\
 Y_{30} &= \left(\frac{7}{4\pi}\right)^{1/2} \frac{1}{2} (5 \cos^3 \theta - 3 \cos \theta) \\
 Y_{3\pm 1} &= \mp \left(\frac{7}{4\pi}\right)^{1/2} \left(\frac{3}{16}\right)^{1/2} \sin \theta (5 \cos^2 \theta - 1) e^{\pm i\phi} \\
 Y_{3\pm 2} &= \left(\frac{7}{4\pi}\right)^{1/2} \left(\frac{15}{8}\right)^{1/2} \sin^2 \theta \cos \theta e^{\pm 2i\phi} \\
 Y_{3\pm 3} &= \mp \left(\frac{7}{4\pi}\right)^{1/2} \left(\frac{5}{16}\right)^{1/2} \sin^3 \theta e^{\pm 3i\phi} \\
 Y_{40} &= \left(\frac{9}{4\pi}\right)^{1/2} \frac{1}{8} (35 \cos^4 \theta - 30 \cos^2 \theta + 3) \\
 Y_{4\pm 1} &= \mp \left(\frac{9}{4\pi}\right)^{1/2} \left(\frac{5}{16}\right)^{1/2} \sin \theta (7 \cos^3 \theta - 3 \cos \theta) e^{\pm i\phi} \\
 Y_{4\pm 2} &= \left(\frac{9}{4\pi}\right)^{1/2} \left(\frac{5}{32}\right)^{1/2} \sin^2 \theta (7 \cos^2 \theta - 1) e^{\pm 2i\phi} \\
 Y_{4\pm 3} &= \mp \left(\frac{9}{4\pi}\right)^{1/2} \left(\frac{35}{16}\right)^{1/2} \sin^3 \theta \cos \theta e^{\pm 3i\phi} \\
 Y_{4\pm 4} &= \left(\frac{9}{4\pi}\right)^{1/2} \left(\frac{35}{2}\right)^{1/2} \frac{1}{8} \sin^4 \theta e^{\pm 4i\phi} \\
 Y_{50} &= \left(\frac{11}{4\pi}\right)^{1/2} \frac{1}{8} (63 \cos^5 \theta - 70 \cos^3 \theta + 15 \cos \theta) \\
 Y_{5\pm 1} &= \mp \left(\frac{11}{4\pi}\right)^{1/2} \left(\frac{15}{2}\right)^{1/2} \frac{1}{8} \sin \theta (21 \cos^4 \theta - 14 \cos^2 \theta + 1) e^{\pm i\phi} \\
 Y_{5\pm 2} &= \left(\frac{11}{4\pi}\right)^{1/2} \left(\frac{105}{32}\right)^{1/2} \sin^2 \theta (3 \cos^3 \theta - \cos \theta) e^{\pm 2i\phi} \\
 Y_{5\pm 3} &= \mp \left(\frac{11}{4\pi}\right)^{1/2} (35)^{1/2} \frac{1}{16} \sin^3 \theta (9 \cos^2 \theta - 1) e^{\pm 3i\phi} \\
 Y_{5\pm 4} &= \left(\frac{11}{4\pi}\right)^{1/2} \left(\frac{315}{2}\right)^{1/2} \frac{1}{8} \sin^4 \theta \cos \theta e^{\pm 4i\phi} \\
 Y_{5\pm 5} &= \mp \left(\frac{11}{4\pi}\right)^{1/2} (7)^{1/2} \frac{3}{16} \sin^5 \theta e^{\pm 5i\phi} \\
 Y_{60} &= \left(\frac{13}{4\pi}\right)^{1/2} \frac{1}{16} (231 \cos^6 \theta - 315 \cos^4 \theta + 105 \cos^2 \theta - 5) \\
 Y_{6\pm 1} &= \mp \left(\frac{13}{4\pi}\right)^{1/2} \left(\frac{21}{2}\right)^{1/2} \frac{1}{8} \sin \theta \\
 &\quad \times (33 \cos^5 \theta - 30 \cos^3 \theta + 5 \cos \theta) e^{\pm i\phi} \\
 Y_{6\pm 2} &= \left(\frac{13}{4\pi}\right)^{1/2} (105)^{1/2} \frac{1}{32} \sin^2 \theta \\
 &\quad \times (33 \cos^4 \theta - 18 \cos^2 \theta + 1) e^{\pm 2i\phi} \\
 Y_{6\pm 3} &= \mp \left(\frac{13}{4\pi}\right)^{1/2} (105)^{1/2} \frac{1}{16} \sin^3 \theta (11 \cos^3 \theta - 3 \cos \theta) e^{\pm 3i\phi} \\
 Y_{6\pm 4} &= \left(\frac{13}{4\pi}\right)^{1/2} \left(\frac{7}{2}\right)^{1/2} \frac{3}{16} \sin^4 \theta (11 \cos^2 \theta - 1) e^{\pm 4i\phi} \\
 Y_{6\pm 5} &= \mp \left(\frac{13}{4\pi}\right)^{1/2} (77)^{1/2} \frac{3}{16} \sin^5 \theta \cos \theta e^{\pm 5i\phi} \\
 Y_{6\pm 6} &= \left(\frac{13}{4\pi}\right)^{1/2} (231)^{1/2} \frac{1}{32} \sin^6 \theta e^{\pm 6i\phi}
 \end{aligned}$$

Table 7b⁴⁰. Spherical Harmonics of order 5 in Cartesian coordinates.

$Y_0^{-5} = \sqrt{\frac{1}{4\pi}}$	$Y_0^{-4} = \sqrt{\frac{9}{4\pi}} \sqrt{\frac{35}{128}} \frac{(x-iy)^4}{r^4}$
$Y_1^{-4} = \sqrt{\frac{3}{8\pi}} \frac{x-iy}{r}$	$Y_1^{-4} = \sqrt{\frac{9}{4\pi}} \sqrt{\frac{35}{16}} \frac{z(x-iy)^3}{r^4}$
$Y_1^{-3} = \sqrt{\frac{3}{4\pi}} \frac{z}{r}$	$Y_2^{-4} = \sqrt{\frac{9}{4\pi}} \sqrt{\frac{5}{32}} \frac{(x-iy)^2}{r^4} (7z^2 - r^2)$
$Y_2^{-4} = -\sqrt{\frac{3}{8\pi}} \frac{x+iy}{r}$	$Y_3^{-4} = \sqrt{\frac{9}{4\pi}} \sqrt{\frac{5}{16}} \frac{(x-iy)}{r^4} (7z^3 - 3zr^2)$
$Y_2^{-3} = \sqrt{\frac{5}{4\pi}} \sqrt{\frac{3}{8}} \frac{(x-iy)^2}{r^3}$	$Y_4^{-4} = \sqrt{\frac{9}{4\pi}} \sqrt{\frac{1}{64}} \frac{35z^4 - 30z^2r^2 + 3r^4}{r^4}$
$Y_3^{-3} = \sqrt{\frac{5}{4\pi}} \sqrt{\frac{3}{2}} \frac{z(x-iy)}{r^3}$	$Y_4^{-3} = -\sqrt{\frac{9}{4\pi}} \sqrt{\frac{5}{16}} \frac{(x+iy)}{r^4} (7z^3 - 3zr^2)$
$Y_4^{-3} = \sqrt{\frac{5}{4\pi}} \sqrt{\frac{1}{4}} \frac{3z^2 - r^2}{r^3}$	$Y_4^{-2} = \sqrt{\frac{9}{4\pi}} \sqrt{\frac{5}{32}} \frac{(x+iy)^2}{r^4} (7z^2 - r^2)$
$Y_4^{-2} = -\sqrt{\frac{5}{4\pi}} \sqrt{\frac{3}{2}} \frac{z(x+iy)}{r^3}$	$Y_4^{-1} = -\sqrt{\frac{9}{4\pi}} \sqrt{\frac{35}{16}} \frac{z(x+iy)^3}{r^4}$
$Y_4^{-1} = \sqrt{\frac{5}{4\pi}} \sqrt{\frac{3}{8}} \frac{(x+iy)^3}{r^3}$	$Y_4^0 = \sqrt{\frac{9}{4\pi}} \sqrt{\frac{35}{128}} \frac{(x+iy)^4}{r^4}$
$Y_4^0 = \sqrt{\frac{7}{4\pi}} \sqrt{\frac{5}{16}} \frac{(x-iy)^3}{r^3}$	$Y_4^1 = \sqrt{\frac{11}{4\pi}} \sqrt{\frac{63}{256}} \frac{(x-iy)^3}{r^3}$
$Y_4^1 = \sqrt{\frac{7}{4\pi}} \sqrt{\frac{15}{8}} \frac{z(x-iy)^2}{r^3}$	$Y_4^2 = \sqrt{\frac{11}{4\pi}} \sqrt{\frac{315}{128}} \frac{z(x-iy)^2}{r^3}$
$Y_4^2 = \sqrt{\frac{7}{4\pi}} \sqrt{\frac{3}{16}} \frac{(x-iy)(5z^2 - r^2)}{r^3}$	$Y_4^3 = \sqrt{\frac{11}{4\pi}} \sqrt{\frac{35}{256}} \frac{(x-iy)^2}{r^3} (9z^2 - r^2)$
$Y_4^3 = \sqrt{\frac{7}{4\pi}} \sqrt{\frac{1}{4}} \frac{z(5z^2 - 3r^2)}{r^3}$	$Y_4^4 = \sqrt{\frac{11}{4\pi}} \sqrt{\frac{105}{32}} \frac{(x-iy)^2}{r^3} (3z^2 - zr^2)$
$Y_4^4 = -\sqrt{\frac{7}{4\pi}} \sqrt{\frac{3}{16}} \frac{(x+iy)(5z^2 - r^2)}{r^3}$	$Y_4^5 = \sqrt{\frac{11}{4\pi}} \sqrt{\frac{15}{128}} \frac{(x-iy)}{r^3} (21z^4 - 14z^2r^2 + r^4)$
$Y_4^5 = \sqrt{\frac{7}{4\pi}} \sqrt{\frac{15}{8}} \frac{z(x+iy)^2}{r^3}$	$Y_4^6 = \sqrt{\frac{11}{4\pi}} \frac{1}{8} \frac{63z^4 - 70z^2r^2 + 15r^4}{r^3}$
$Y_4^6 = -\sqrt{\frac{7}{4\pi}} \sqrt{\frac{5}{16}} \frac{(x+iy)^3}{r^3}$	$Y_4^7 = -\sqrt{\frac{11}{4\pi}} \sqrt{\frac{15}{128}} \frac{z+iy}{r^3} (21z^4 - 14z^2r^2 + r^4)$
	$Y_4^8 = \sqrt{\frac{11}{4\pi}} \sqrt{\frac{105}{32}} \frac{(x+iy)^3}{r^3} (3z^2 - zr^2)$
	$Y_4^9 = -\sqrt{\frac{11}{4\pi}} \sqrt{\frac{35}{256}} \frac{(x+iy)^2}{r^3} (9z^2 - r^2)$
	$Y_4^{10} = \sqrt{\frac{11}{4\pi}} \sqrt{\frac{315}{128}} \frac{z(x+iy)^2}{r^3}$
	$Y_4^{11} = -\sqrt{\frac{11}{4\pi}} \sqrt{\frac{63}{256}} \frac{(x+iy)^2}{r^3}$
	$Y_4^{12} = \sqrt{\frac{11}{4\pi}} \sqrt{\frac{63}{256}} \frac{(x+iy)^3}{r^3}$

CHAPTER 3EXPERIMENTAL PROCEDURESPART IPREPARATIONS OF THE REAGENTS

The reagents needed for the synthesis of the compounds were anhydrous nickel (II) chloride, anhydrous cobalt (II) chloride, anhydrous nickel (II) bromide, anhydrous cobalt (II) bromide, acetonitrile-boron trichloride, acetonitrile-boron tribromide, anhydrous acetonitrile and anhydrous toluene. These reagents had to be prepared from the beginning because the anhydrous metal halides and the acetonitrile boron trihalides were not commercially available. The stock chemicals needed to prepare the above reagents were hexahydrated nickel (II) chloride, hexahydrated cobalt (II) chloride, nickel metal finings, cobalt (II) carbonate, thionyl chloride, hydrobromic acid, boron trichloride, boron tribromide, acetonitrile and toluene.

(1) Preparation of Anhydrous Nickel (II) Chloride from Hexahydrated Nickel (II) Chloride.

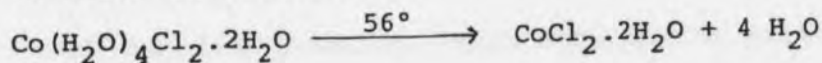
The method of preparation of this anhydrous nickel (II) chloride was developed by Pray⁴¹. The hydrated nickel (II) chloride was to react with thionyl chloride to produce the anhydrous chloride.

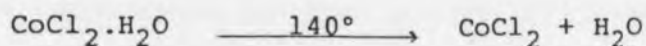
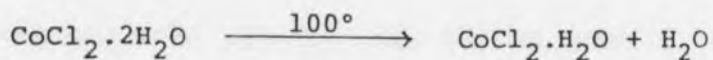


55 gram of finely ground hexahydrated nickel (II) chloride was placed in a 250 ml round bottom flask. 100 ml of freshly distilled thionyl chloride was added to the flask and reaction was carried out under a hood. After the evolution of the gases had subsided, the slurry was refluxed for 2 hours and the contents were cooled to room temperature under a nitrogen atmosphere. A 30 ml portion of fresh thionyl chloride was syringed into the flask to test for completeness of the reaction. The slurry was again refluxed for two more hours and then cooled to room temperature under nitrogen. Excess thionyl chloride was distilled off and the product was dried on a high vacuum line for 24 hours. The dried product was transferred to a vacuum desiccator containing potassium hydroxide and was stored under nitrogen in the desiccator for a minimum of 48 hours to remove traces of thionyl chloride. The product weighed 29 grams. The yield was 97%.

(2) Preparation of Anhydrous Cobalt (II) Chloride

The procedure described by Pray could be applied for this synthesis, but there was another much simpler approach. From the properties described in the Merck Index⁴², the anhydrous cobalt (II) chloride could be prepared by direct heating of the hexahydrated cobalt (II) chloride in vacuum.

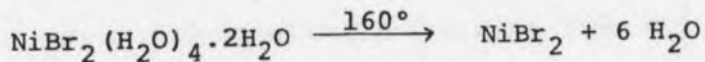




50 grams of finely ground hexahydrated cobalt (II) chloride and a magnetic stirring bar were placed in a 250 ml round bottom flask. The latter was attached to a high vacuum line and evacuated. Under slow stirring, the flask was heated in an oil bath at 142°. The water vapor from the decomposition of the hexahydrated cobalt (II) chloride had changed to pale blue when the dehydration was completed. The anhydrous compound weighed 23 grams. The yield was 87%.

(3) Preparation of Anhydrous Nickel (II) Bromide

The method of preparation of anhydrous nickel (II) bromide was a slight modification to the procedure described previously by Ward⁴³.

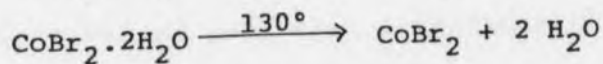
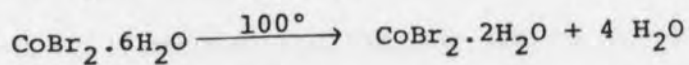


10 grams of nickel metal fining were placed in a crucible and heated strongly in open air for about 30 minutes with constant stirring. The black nickel oxide powder was then transferred to a beaker containing 25 ml of 47% hydrobromic acid and 5 ml of distilled water. With stirring, the reaction mixture was heated up to 85° under a hood. About 0.1 gram of nickel metal finings was added to react with the free bromine. When most of the solid

had dissolved, the solution was boiled briefly, cooled to room temperature and then gravity filtered. The filtrate was vigorously evaporated with stirring and an impinging stream of compressed air. When the solution was concentrated, the yellowish-green needles of the hydrated nickel (II) bromide precipitated. The product was collected by suction filtration and dried in a circulating air oven for an hour at about 95°. The ground product was put in a 250 ml round bottom flask with a magnetic stirring bar. The flask was attached to a high vacuum line and with slow stirring, the contents heated to 160° in an oil bath. The dehydration was completed when the color changed from yellowish-green to orange-yellow. The compound weighed 32 grams and the yield was 76%.

(4) Preparation of Anhydrous Cobalt (II) Bromide

Anhydrous cobalt (II) bromide could be prepared via hexahydrated cobalt (II) bromide from cobalt (II) carbonate and hydrobromic acid⁴⁴ or from cobalt (II) acetate and acetyl bromide⁴⁵ or from cobalt (II) oxide and hydrobromic acid⁴³. The method I employed was the reaction between cobalt (II) carbonate and the hydrobromic acid.



20 grams of cobalt (II) carbonate was mixed with 40 ml 47% hydrobromic acid and 15 ml of distilled water. The carbonate dissolved and carbon dioxide evolved. The violet-pink solution was gravity filtered and vigorously evaporated with an impinging stream of compressed air to near dryness. After it cooled to room temperature, a violet-pink solid crust formed. The solid was crushed and put into a 250 ml round bottom flask with a magnetic stirrer. Then the flask was attached to a high vacuum line and evacuated. With slow stirring, the content was heated in an oil bath at a temperature slightly higher than 130°. This was the total dehydration temperature of the hexahydrated cobalt (II) bromide. The anhydrous cobalt (II) bromide was bright green in color and weighed 30 grams, and the percent yield was 81%.

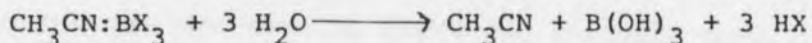
(5) Preparation of Acetonitrile Boron Trihalide Adducts



X = halides (Cl^-/Br^-)

Acetonitrile boron trihalide adducts were the chief reactants for the preparations of the nickel (II) and cobalt (II) complexes. Upon reaction with anhydrous metal halide in a mixed solvent of acetonitrile and toluene, the covalent bond in the adduct cleaved and acetonitrile formed the ligands around the metal cation. The free halide ions then combined with boron trihalides

to form the tetrahaloborate anion. The adducts were extremely air and moisture sensitive; therefore, the synthesis had to be carried out in an inert atmosphere.



The boron trihalides and acetonitrile were polar compounds and the solvent needed for this preparation had to be polar, but also it must be nonreactive to either of the reagents. Toluene possessed all the properties above and it was chosen to be the inert solvent for this purpose.

(A) Distillation of Acetonitrile or Toluene

0.7 liter of reagent grade acetonitrile or toluene was put into a 1-liter round bottom flask containing 2.00 grams of calcium hydride as drying agent. Calcium hydride would remove the water from the solvent as hydrogen gas and calcium hydroxide. The solvent was then distilled under nitrogen and stored over Linde 4°A molecular sieves in a 1-liter Schlenk flask.

(B) Preparation of Acetonitrile Boron Trichloride Adduct



This procedure was a major modification of the one used by Haworth⁴⁶.

A 1-liter three-neck flask was equipped with a pressure equalizing addition funnel. One of the openings was connected to a T-joint which delivered a gaseous

mixture of nitrogen and boron trichloride. The last opening and the addition funnel were directly connected to a high vacuum line. A small amount of the boron trichloride gas was used to flush the delivery tube. The experimental setup was evacuated and flushed with nitrogen for several times. 20 ml of anhydrous acetonitrile (wt. = 14 gm., $d = 0.7138$)⁴⁷ was syringed into the addition funnel under positive nitrogen pressure. At the same time, 0.15 liter of anhydrous toluene was also added to the funnel. The three neck flask was then evacuated and lowered into a dry ice and acetone bath. The reaction was exothermic when the adduct was formed. The cold bath served as a reservoir to extract the heat from the reaction. Boron trichloride gas liquified below 12° ⁴⁸. The gas was slowly released into the flask until a volume of 31.00 ml (wt. = 43 gm., $d = 1.3728$)⁴⁸ had been condensed in the flask, then boron trichloride gas flow was stopped and then replaced by nitrogen. The nitrogen gas pressure was kept slightly above the atmospheric pressure. The mixed solvents (toluene and acetonitrile) were run into the flask at a slow rate. As soon as the reagents contacted each other, a white precipitate was formed. The adduct was transferred to a fritted filter funnel under nitrogen and the excess solvents were being filtered away into a receiver. The product was dried on the vacuum line for 24 hours. The adduct weighed 55 grams and the percent yield was 97%.

(C) Preparation of Acetonitrile Boron Tribromide Adduct

Very similar to boron trichloride, boron tribromide decomposed to boric acid and hydrogen bromide upon exposure to moisture in the air.



Air-free technique had to be applied to this synthesis. The experimental setup was similar to that of the preparation of acetonitrile boron trichloride adduct but with minor differences. At room temperature, boron tribromide was a liquid.

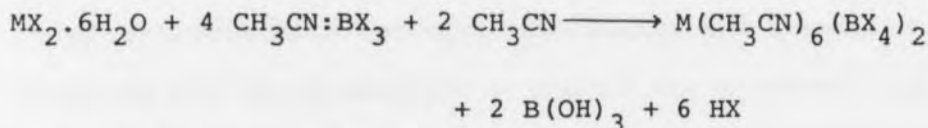
A 1-liter three neck flask was equipped with a stop-cock, which served as nitrogen gas flow control, was attached to one opening. The remaining opening was connected to a high vacuum line with a stop-cock. The setup was evacuated and flushed with nitrogen at least 10 times to ensure it was air free. Then under a stronger nitrogen gas flow, 16 ml (wt. = 43 gm., $d = 2.6431$)⁴⁷ of boron tribromide was transferred to the funnel from the dry box by a syringe. A mixture of 10 ml anhydrous acetonitrile (7 gm.) and 40 ml of anhydrous toluene was also syringed into the flask simultaneously. The system was lowered into a dry ice and acetone bath. When it was thoroughly chilled, boron tribromide was added slowly to the solvent mixture and a white precipitate was formed. The reaction of acetonitrile and boron tribromide was

exothermic and the dry ice bath served as the heat sink. The product was collected in a fritted filter funnel under nitrogen and was dried on the vacuum line for 24 hours. The adduct weighed about 47 grams and the yield was 63%.

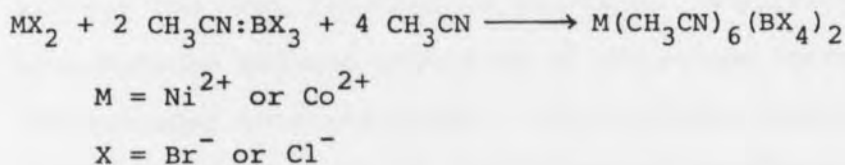
PART II

Synthesis of Transition Metal Complexes $M(\text{CH}_3\text{CN})_6(\text{BX}_4)_2$

The complexes could be prepared either by the hydrated metal halides



or by the anhydrous metal halides.

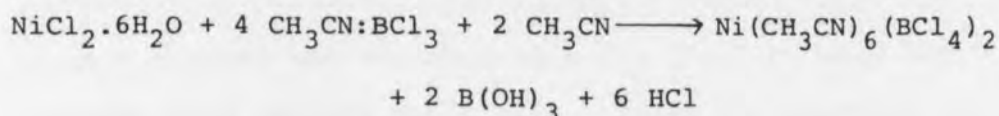


The experimental conditions and the setup were exactly the same for all four compounds, hexa(acetonitrile)nickel (II) tetrachloroborate ($\text{Ni}(\text{CH}_3\text{CN})_6(\text{BCl}_4)_2$), hexa(acetonitrile)cobalt(II) tetrachloroborate ($\text{Co}(\text{CH}_3\text{CN})_6(\text{BCl}_4)_2$), hexa(acetonitrile)nickel(II) tetrabromoborate ($\text{Ni}(\text{CH}_3\text{CN})_6(\text{BBr}_4)_2$) and hexa(acetonitrile)cobalt(II) tetrabromoborate ($\text{Co}(\text{CH}_3\text{CN})_6(\text{BBr}_4)_2$).

In the following sections, only the synthesis of hexa(acetonitrile)nickel(II) tetrachloroborate from both hydrated

and anhydrous nickel(II) chloride would be given.

(1) Preparation of Hexa(acetonitrile)nickel(II) Tetrachloro-
borate Complexes using Hexahydrated Nickel(II) Chloride

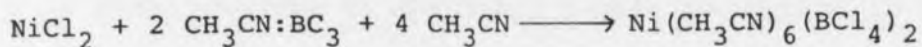


A thoroughly dried 150 ml three neck flask was flushed with nitrogen continuously. About 14 grams of acetonitrile borontrichloride adduct was weighed out in the dry box and was transferred to the flask. The flask was sealed off under nitrogen with two stopcock joints and a stopper. Nitrogen gas was connected to one of the stopcock joints and the pressure was regulated until the standard taper stopper was just floating in the neck. A mixture of 20 ml of anhydrous toluene and 10 ml of anhydrous acetonitrile was syringed into the flask. The nitrogen flow was increased and 5 grams of finely ground hexahydrated nickel(II) chloride was quickly introduced into the flask through a powder funnel, together with a magnetic stirring bar. The stopper was then replaced back in its original position. The other stopcock joint was connected to a U-shaped bubbler containing concentrated ammonium hydroxide to trap the hydrogen chloride generated from the reaction. Under a slow flow of nitrogen gas, the reaction mixture was stirred until all the nickel(II) chloride was consumed. As the reactants mixed together,

a white precipitate and a purple-blue precipitate were formed. The white precipitate was boric acid and the purple-blue precipitate was the nickel complexes. Another 10 ml portion of 1:1 anhydrous acetonitrile and toluene mixture was syringed into the flask to keep the contents from getting too slushy. After the reaction was over, the stopper was replaced by a long stem condenser and again, a 10 ml portion of anhydrous acetonitrile was syringed into the flask to ensure acetonitrile was present in excess. The content was refluxed under nitrogen for one hour to drive off the absorbed hydrogen chloride in the mixture. The complexes were redissolved in the hot solvent to effect separation from boric acid. The hot solution was transferred under nitrogen into an extractor which had previously been flushed with nitrogen. After the solution had dripped through the fritter filter into the receiver, the solution was refluxed again and the solvent vapor extracted the absorbed complexes into the receiver. The extraction was completed when the remaining boric acid was white. The flask was cooled to room temperature under nitrogen and then attached to a high vacuum line. The solution was concentrated and the product precipitated. The product was transferred to a fritted filter funnel under nitrogen and dried on the vacuum line for 24 hours. The purple-blue

hexa(acetonitrile)nickel(II) tetrachloroborate weighed 9 grams and the yield was 67%.

(2) Preparation of Hexa(acetonitrile)nickel(II) Tetrachloroborate Complexes using Anhydrous Nickel(II) Chloride



Hexahydrated nickel(II) chloride had a fair solubility in acetonitrile, but anhydrous nickel(II) chloride dissolved to a very small extent. The reaction was run at 50°.

A 250 ml three neck flask equipped with a condenser and a magnetic stirring bar was thoroughly cleaned and flushed with nitrogen gas. 3 grams (0.0231 mole) of anhydrous nickel(II) chloride and 7 grams (0.0462 mole) of acetonitrile adduct were introduced into the flask through a powder funnel under a stronger nitrogen flow. 10 ml (wt. = 7 gm., $d = 0.7138$)⁴⁷ of anhydrous acetonitrile and 40 ml anhydrous toluene was syringed into the flask. The flask was lowered into a warm water bath and the temperature was maintained at 60°. Under nitrogen and at constant temperature, the reacting materials were stirred for several hours until all the nickel chloride had consumed. The contents were transferred to an extractor under nitrogen and went through the same extraction process described previously. The purple-blue complexes weighed 12 grams and the yield was 79%.

The color of the complexes, hexa(acetonitrile) cobalt(II) tetrachloroborate ($\text{Co}(\text{CH}_3\text{CN})_6(\text{BCl}_4)_2$), prepared from anhydrous cobalt(II) chloride were pinkish brown and the crystal formed perfect transparent hexagons. A small portion of the solid slowly decomposed in the storage container and the color changed to sky-blue. Upon several purifications, the color of the complexes changed to sky-blue. But the color of the same complex, when prepared from the hydrated cobalt(II) chloride, was sky-blue.

The color of the complexes, hexa(acetonitrile) nickel(II) tetrabromoborate ($\text{Ni}(\text{CH}_3\text{CN})_6(\text{BBr}_4)_2$) was greyish-purple and that of hexa(acetonitrile)cobalt(II) tetrabromoborate ($\text{Co}(\text{CH}_3\text{CN})_6(\text{BBr}_4)_2$) was apple-green. All these complexes were prepared from their corresponding anhydrous metal bromides. Experimental setups were shown in figures 4 and 5.

Part III

(1) Thermal Analyses Procedure

In this experiment, the thermal analysis equipment used was the TGS-1 thermal balance and the Perkin-Elmer DSC-1b differential scanning calorimeter. Because of the extreme air sensitivity of the materials involved, and special demands of the analog data output, some modifications of the thermal balance and the operating

procedures were necessary. Bratten⁴⁹ gave detailed descriptions of the major modifications of the equipment, and the sample handling techniques in his thesis. In DSC experiments, micro-metal crucibles were used. The sample size was about 5 mg. Preweighed crucibles and lids were transferred to the dry box, and small samples were loaded into the crucibles. The lids and the crucibles were hermetically sealed. Each crucible was labeled to identify the complex and then reweighed. The sample weight was obtained by taking the difference of the two weighings. The sample holder of the DSC-1b were two small electrically heated brass plates. The carrier gas was argon. A large hollowed cylinder was placed over the heaters, and the carrier gas was allowed to flood the cylinder to expel the air. The crucible which contained the sample was placed in the heater, and small pin holes were punched on the surface. This would allow volatiles to escape during heating. Then the sample holder was isolated in a pure argon atmosphere with a special cover provided with the instrument. The heating rate was set at 10° per minute and the range was set at 8 μ -cal full scale. The DSC curves were recorded on a strip chart and the digital data were recorded on paper tapes. The System 72 computer in the Chemistry Department was used in calculations. (See appendix for a listing of the program).

(2) X-ray Analyses Procedures

Samples were loaded into 0.05 mm thin walled capillary tubes in the dry box and sealed with vacuum grease. The capillary was placed in the middle of the camera and the X-ray film was loaded into the camera in a dark box. The camera was then mounted onto the X-ray machine and the exposure time was 6 to 8 hours. The radiation used was Ni filtered Cu (K_2).

(3) Infrared Analyses Procedures

Samples were prepared in nujol mull in the dry box. Standard NaCl salt plates were used. The infrared spectra were recorded on a Perkin-Elmer Infrared Spectrometer under ordinary atmosphere. More recent spectra were recorded under nitrogen atmosphere and in KBr pellets.

(4) Ligand-field Analyses Procedures

Samples were prepared in a nitrogen glove bag. Cold anhydrous acetonitrile was used as solvent. The complex solution was transferred to the spectral cell by a syringe. Spectra were recorded on the DK-Beckman 2A UV-Visible Spectrometer at room temperature. Spectral region scanned was from the near infrared to the visible. Precipitates formed from the solution very quickly at low temperatures and spectra were not obtained.

CHAPTER 4
RESULTS AND DISCUSSIONS

Elemental Analysis

The elemental analysis is to find the number of ligands bonded to the transition metal and the number of boron atoms in the counter-ion. The experimental and calculated values are compared for the same model. The compounds were sent to Galbraith Laboratories* for carbon, hydrogen, nitrogen and boron analysis. The results of the experimental analysis (see Table 8) are close to but somewhat different from the theoretical calculations (see Table 9), which are based on the formulae shown. No corrections have been made to these tables with regard to the impurity. Only the last compound in the series, $\text{Co}(\text{CH}_3\text{CN})_6(\text{BBr}_4)_2$, poses some serious problem. After trying several different models, it is found from the low C, H, N percentage to be a three coordinated species. The next task is to calculate the percentages of the elements with inclusion of the impurity, boric acid; the ratio of the complexes to the impurity is assumed to be 1:1. The new values are found to be in much closer agreement with the experimental values. The low percentages of boron in the first complex, $\text{Ni}(\text{CH}_3\text{CN})_6(\text{BCl}_4)_2$ has no evident explanation.

	<u>% C</u>	<u>% H</u>	<u>% N</u>	<u>% B</u>	mole ratio
					Ligand/ Boron
Ni(CH ₃ CN) ₆ (BBr ₄) ₂	14.42	1.96	8.37	1.75	3.80
Co(CH ₃ CN) ₆ (BCl ₄) ₂	21.34	3.11	12.99	4.45	2.25
Ni(CH ₃ CN) ₆ (BCl ₄) ₂	21.86	3.13	12.98	4.43	2.29
Co(CH ₃ CN) ₆ (BBr ₄) ₂	8.10	1.09	4.66	3.87	0.96

Table 8. Elemental analysis* of the percentages of C, H, N and B in the complexes.

	<u>% C</u>	<u>% H</u>	<u>% N</u>	<u>% B</u>	mole ratio
					Ligand/ Boron
Ni(CH ₃ CH) ₆ (BBr ₄) ₂	14.92	1.87	8.70	2.24	3.0
Co(CH ₃ CN) ₆ (BCl ₄) ₂	23.59	2.95	13.76	3.54	3.0
Ni(CH ₃ CN) ₆ (BCl ₄) ₂	23.60	2.95	13.76	3.54	3.0
Co(CH ₃ CN) ₆ (BBr ₄) ₂	14.91	1.86	8.70	2.24	2.0

Table 9. Theoretical calculated elemental analysis of the percentages of C, H, N and B in the complexes.

*The results of this elemental analysis were done by Galbraith Laboratories, Inc., Knoxville, Tennessee 37921.

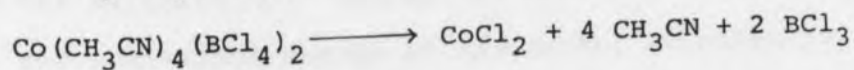
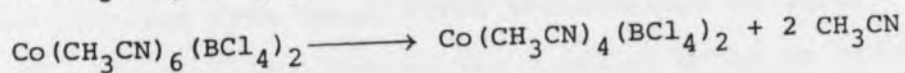
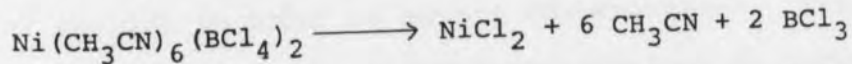
	mole ratio				
	Ligand/ Boron				
	<u>% C</u>	<u>% H</u>	<u>% N</u>	<u>% B</u>	<u>Boron</u>
$\text{Ni}(\text{CH}_3\text{CN})_6(\text{BBr}_4)_2$	14.01	2.04	8.17	3.21	2.02
$\text{Co}(\text{CH}_3\text{CN})_6(\text{BCl}_4)_2$	21.40	3.12	12.48	4.90	2.02
$\text{Ni}(\text{CH}_3\text{CN})_6(\text{BCl}_4)_2$	21.43	3.13	12.51	4.83	2.06
$\text{Co}(\text{CH}_3\text{CN})_6(\text{BBr}_4)_2$	7.95	1.33	4.46	3.64	1.01

Table 10. Theoretical calculated values of the percentages of C, H, N and B in the complexes with the inclusion of $\text{B}(\text{OH})_3$.

By comparing tables 8 and 10, we are quite safe to say that the complexes, $\text{Ni}(\text{CH}_3\text{CN})_6(\text{BCl}_4)_2$, $\text{Co}(\text{CH}_3\text{CN})_6(\text{BCl}_4)_2$, $\text{Ni}(\text{CH}_3\text{CN})_6(\text{BBr}_4)_2$ are of coordination 6 whereas $\text{Co}(\text{CH}_3\text{CN})_6 \cdot (\text{BBr}_4)_2$ is a 3 coordinated species.

Thermal Decomposition Analysis

In thermal decomposition experiments, the complexes break down due to heating in a thermal balance or in a differential scanning calorimeter. The possible products of the decomposition are metal halides, acetonitrile and boron trihalides. The process may involve a single step decomposition or a multiple step decomposition. The DTG and DSC curves for $\text{Ni}(\text{CH}_3\text{CN})_6(\text{BCl}_4)_2$ were single peaked which indicated the thermal decomposition of this complex was a single step process. The DTG peak maxima appeared at about 106° and the DSC peak maxima appeared at about 168° . Whereas the DTG and DSC curves for $\text{Co}(\text{CH}_3\text{CN})_6(\text{BCl}_4)_2$ were double peaked which indicated the decomposition involved a two step process. In the DTG curve, the first peak appeared at about 120° and the second appeared at about 135° . In the DSC curve, the first peak was located at 135° and the second was at 158° . From the weight loss appearing on the DTG curve, the cobalt complex seemed to change the coordination from 6 to 4 in the first step and from 4 to 0 in the second.



Both TG/DTG and DSC analyses are used to study the activation energies and the order of the reactions of the compounds. In the DTG analysis, there are three models of calculating the activation energy and the order of the reaction. The first model is the Freeman-Carrol⁵⁰ calculation, the second model is the Tang⁵¹ calculation and the third model is the Coates-Redfern⁵² calculation. By comparing the results obtained from the calculations (see Table 12), we can see that the nickel complex has a higher activation energy than the cobalt complex. This result is reasonable because the complexes have equal numbers of identical ligands and counterions and only the transition metal is different. If the effective nuclear charges on Ni(II) are stronger than Co(II), then Ni(II) can attract the lone pair of electrons or the ligand stronger than Co(II). As a result, the ligand-metal bond in nickel complexes is stronger. This results in a more stable structure for the nickel complex. To break the coordination bonds in these complexes in the thermal decomposition reaction, we will expect to provide more energy to the nickel complex in order to effect decomposition. The values obtained from these three calculations do agree with the expectation. Taking the reaction order as being one, the activation energy of the nickel reaction is 20.50 kcal/mole and that of the cobalt reaction is 15.23 kcal/mole.

The DSC is used to confirm a reaction. The DSC curves show that the thermal decomposition of the nickel complex is a single step reaction whereas the decomposition of the cobalt complex is a two step reaction. This same phenomena for the cobalt reactions are also observed in the TG/DTG analysis. In the DSC kinetic analysis, the heat of reaction is measured. From the heat of reaction, the activation energy, the reaction order, and the correlation coefficients can be computed. These correlation coefficients serve as a measure of the linearity of the Arrhenius activation energy plot and help to pick out the best reaction order and the activation energy for the reaction. Theoretically, the two analyses should present the same results, but we find the values of the activation energy are different. The DSC kinetic analysis presents a much higher activation energy. The large differences in the activation energy are due to the equipment configurations for the two analyses. In the DTG analysis, we use an open micro-crucible, and a constant flow of carrier gas, helium, sweeps the volatiles away from the crucible during heating. This prevents the volatiles from depositing in the crucible. In DSC experiments, the volatiles are more confined in the crucible which creates a thermal barrier for the system and results in a higher activation energy. Even though the DSC kinetics measurements have a higher value than the DTG measurements, they are in agreement with each

other than $\text{Ni}(\text{CH}_3\text{CN})_6(\text{BCl}_4)_2$ has a higher activation energy than $\text{Co}(\text{CH}_3\text{CN})_6(\text{BCl}_4)_2$. The nickel complex is a more stable compound.

	<u>Activation Energy in kcal/mole</u>	<u>Order of Reaction</u>	<u>Correlation Coefficient</u>
$\text{Ni}(\text{CH}_3\text{CN})_6(\text{BCl}_4)_2$			
DSC Kinetics	35.49	1	0.99991
DTG C - R	20.47	1	0.99954
$\text{Co}(\text{CH}_3\text{CN})_6(\text{BCl}_4)_2$			
DSC Kinetics	23.67	1	0.99117
DTG C - R	15.23	1	0.99833

Table 11. Comparison between DSC and DTG data.

TG/DTG and DSC curves were shown in figures 6 through 9.

<u>Freeman-Carrol Calculation</u>	<u>Activation Energy in kcal/mole</u>	<u>Order of Reaction</u>	<u>Correlation Coefficient</u>
Ni(CH ₃ CN) ₆ (BCl ₄) ₂	17.97	1/2	0.99970
Co(CH ₃ CH) ₆ (BCl ₄) ₂	16.07	2/3	0.99834

<u>Tang Calculation</u>	<u>Activation Energy in kcal/mole</u>	<u>Order of Reaction</u>	<u>Correlation Coefficient</u>
Ni(CH ₃ CN) ₆ (BCl ₄) ₂	22.54		0.99699
Co(CH ₃ CN) ₆ (BCl ₄) ₂	18.25		0.99953

<u>Coates-Redferns Calculation</u>	<u>Activation Energy in kcal/mole</u>	<u>Order of Reaction</u>	<u>Correlation Coefficient</u>
Ni(CH ₃ CN) ₆ (BCl ₄) ₂	16.05	0	0.99857
	18.14	1/2	0.99989
	18.89	2/3	0.99995
	20.47	1	0.99954
Co(CH ₃ CN) ₆ (BCl ₄) ₂	12.53	0	0.99985
	13.83	1/2	0.99950
	14.28	2/3	0.99919
	15.23	1	0.99833

Table 12. TG/DTG data of the complexes Ni(CH₃CN)₆(BCl₄)₂ and Co(CH₃CN)₆(BCl₄)₂.

X-ray Powder Analysis

The X-ray powder diffraction method is not very useful for complicated molecules. It is only good for simple cubic, body-centered and face-centered cubic structures. Even though the method is not very powerful for structural analysis, it still provides some useful information. If we look at Table 13, the d values for both $\text{Ni}(\text{CH}_3\text{CN})_6(\text{BCl}_4)_2$ and $\text{Co}(\text{CH}_3\text{CN})_6(\text{BCl}_4)_2$ are strikingly similar, the line intensities do correspond to each other exactly. We can conclude that the crystal structures for the two complexes are extremely similar or they may be identical. From the ratio of the smallest $1/d^2$ to other $1/d^2$ values, the closest structure we can propose is the trigonally distorted calcium fluoride crystal. When we look at the data for $\text{Ni}(\text{CH}_3\text{CN})_6(\text{BBr}_4)_2$ and $\text{Co}(\text{CH}_3\text{CN})_6(\text{BBr}_4)_2$, the patterns are not similar at all. There are only 5 d values that appear to be common to both species. With the aid of the elemental analysis, we can rule out the possibility that both species are six-coordinated. If we compare $\text{Ni}(\text{CH}_3\text{CN})_6(\text{BBr}_4)_2$ with $\text{Ni}(\text{CH}_3\text{CN})_6(\text{BCl}_4)_2$, again we see a general similar diffraction pattern. We can assume this is also a trigonally distorted octahedron. This indicates that the last complex is not six-coordinated. The structure cannot be obtained from the X-ray analysis. Reedink⁵³ indicated these compounds were isomorphous. There is a strong belief that the complex for cobalt,

$\text{Co}(\text{CH}_3\text{CN})_6(\text{BBr}_4)_2$ should be six-coordinated rather than three-coordinated. The reason for this belief is that the freshly prepared compound was deep-apple green. When the X-ray analysis was performed on this compound, the color had changed to yellow-green. That indicated the compound might have decomposed to some extent. The strong suspicion for the decomposition of these compounds came from the fact that the dry box had malfunctions during the course of analyses. That the atmosphere of the dry box had been contaminated with moisture was highly possible. The decomposition of the compounds was more evident from the IR and ligand field spectra. The X-ray data are given in Table 13.

I o		II o		III o		IV o	
d	I	d	I	d	I	d	I
5.80	s	5.80	s	10.00	m	6.00	
4.90	w	4.10	s	7.50	m	5.30	
4.10	s	3.75	m	5.80	s	5.00	
3.75	m	3.60	s	4.80	w	4.05	
3.60	s	3.35	m	4.20	m	3.40	
3.35	m	3.17	s	3.90	m	3.25	
3.15	s	2.90	m	3.75	s	2.84	
3.10	s	2.80	s	3.25	s	2.80	
2.90	m	2.70	m	2.95	s	2.75	
2.80	s	2.60	w	2.85	s	2.70	
2.75	w	2.50	m	2.75	w	2.65	
2.70	m	2.45	w	2.55	s	2.33	
2.57	m	2.30	m	2.35	s	2.24	
2.50	m	2.25	m	2.30	s	2.17	
2.45	w	2.20	w	2.25	w	2.05	
2.30	m	2.15	w	2.20	s	2.03	
2.25	m	2.13	w	2.10	w	2.00	
2.18	w	2.09	w	2.05	w	1.96	
2.13	w	1.98	w	1.98	m	1.86	
2.09	w	1.90	w	1.86	m	1.73	
2.04	w	1.80	m	1.78	w	1.66	
1.96	w	1.67	m	1.72	m	1.63	
1.90	w	1.61	m	1.64	m	1.55	
1.80	m	1.60	m	1.55	m	1.53	
1.67	m	1.58	w	1.52	w	1.43	
1.61	m			1.48	w		
1.60	m						
1.56	w						
1.47	w						

d = crystal plane distance
I = intensity, s = strong
w = weak, m = medium

Table 13. X-ray powder diffraction patterns for the compounds. Compound I is $\text{Ni}(\text{CH}_3\text{CN})_6(\text{BCl}_4)_2$, Compound II is $\text{Co}(\text{CH}_3\text{CN})_6(\text{BCl}_4)_2$, Compound III is $\text{Ni}(\text{CH}_3\text{CN})_6(\text{BBr}_4)_2$ and Compound IV is $\text{Co}(\text{CH}_3\text{CN})_6(\text{BBr}_4)_2$.

Infrared Analysis

The acetonitrile molecule belongs to point group C_{3v} and it has eight normal modes of vibrations. v_1 to v_4 are symmetrical and belong to the A_1 species; v_5 to v_8 are degenerate and belong to the E species. The infrared spectra of acetonitrile coordinated to metal cations had been fully analyzed by Reedijk et al¹⁶. The modes of vibrations, the frequencies of the fundamentals, the most important combination and overtone bands of acetonitrile and also the shift-ranges when it is coordinated to metal ions are listed in Table 14.

	<u>Free Ligand</u>	<u>Ni(CH₃CN)₆²⁺</u>	<u>Co(CH₃CN)₆²⁺</u>
v_2	2254 cm ⁻¹	2302 cm ⁻¹	2295 cm ⁻¹
v_3	1376 cm ⁻¹	1369 cm ⁻¹	1370 cm ⁻¹
v_4	917 cm ⁻¹	948 cm ⁻¹	945 cm ⁻¹
$v_3 + v_4$	2293 cm ⁻¹	2332 cm ⁻¹	2323 cm ⁻¹
v_7	1047 cm ⁻¹	1034 cm ⁻¹	1035 cm ⁻¹
$2v_4 + v_8$	2204 cm ⁻¹	2263 cm ⁻¹	2255 cm ⁻¹
$2v_8$	749 cm ⁻¹	785 cm ⁻¹	777 cm ⁻¹
v_8	379 cm ⁻¹	406 cm ⁻¹	402 cm ⁻¹

Table 14¹⁶. Comparison of the IR frequency shifts between the free ligands and the complexes.

The nitrile stretching frequency shifted to higher frequencies were observed. The lack of splitting of the CN stretching absorption peaks indicated the ligands were coordinated in the same manner. The characteristic water peak appeared at around 3600 cm^{-1} in all spectra, indicating that compounds had decomposed partially to boric acid. Another absorption peak appeared at 2260 cm^{-1} showing that there was uncoordinated acetonitrile absorbed in the compound. The decomposition of the compounds was probably due to the presence of moisture in the dry box and the container. The peak due to the presence of free ligands could be explained in terms of the liberation of acetonitrile from the compound during decomposition. In the process of purifications and recrystallizations of the compounds from acetonitrile, it was very likely that free acetonitrile molecules were absorbed in the crystal lattice. The presence of these impurity peaks makes the identification of the peaks for the complexes difficult in my preparations.

Ligand-field Analysis

The ligand-field spectra of completely solvated Ni^{2+} and Co^{2+} ions with acetonitrile in an octahedral environment had been previously reported by Wickenden and Krause⁵⁴ and Reedijk and Groeneveld⁵⁵. In the nickel complexes spectra, four major peaks are found. The first band is assigned to ${}^3A_{2g} \rightarrow {}^3T_{2g}$ and is found in the region of $7000\text{-}12000\text{ cm}^{-1}$,

the second is assigned to $3_{A_{2g}} \rightarrow 3_{T_{1g}}$ (F) and appears in the region 12000-20000 cm^{-1} . The third band appears in the region of 21000-30000 cm^{-1} and belongs to $3_{A_{2g}} \rightarrow 3_{T_{1g}}$ (P) transition. A weak spin forbidden transition, $3_{A_{2g}} \rightarrow 1_{E_g}$ is located in the region of 11500-15500 cm^{-1} . The $3_{A_{2g}} \rightarrow 3_{T_{2g}}$ transition is taken as 10 Dq, the crystal field splitting energy. This band is difficult to determine for weak ligands because it is in the near-infrared region and the band maximum is often hampered by infrared overtones due to the vibrations of the ligands. The Co(II) ligand-field spectra of octahedral species should consist of three strong bands and a weak one. The three strong bands are assigned to $4_{T_{1g}}$ (F) \rightarrow $4_{T_{2g}}$, $4_{T_{1g}} \rightarrow 4_{A_{2g}}$ and $4_{T_{1g}}$ (F) \rightarrow $4_{T_{1g}}$ (P), the weaker one being the spin forbidden transition. This spin forbidden band is not observed frequently. The 10 Dq value is obtained from the $4_{t_{1g}}$ (F) \rightarrow $4_{T_{2g}}$. But in our ligand-field spectra, none of the features confirm the reported values. The spectrum has numerous complexed bands with multiple splittings. To judge the validity of decomposition of the compound, a spectrum of anhydrous CoCl_2 in wet acetonitrile was obtained and the result was compared with the spectrum of the complex, $\text{Co}(\text{CH}_3\text{CN})_6(\text{BCl}_4)_2$, the features on these two spectra were identical. From this, I concluded the compounds had decomposed and the evaluation of the spectra was inclusive.

SUMMARY

This study has dealt with the synthesis and the characterization of Ni(II) and Co(II) complexes having the general formula $M(\text{CH}_3\text{CN})_6(\text{BX}_4)_2$ where X is either bromide or chloride.

Cobalt(II) and nickel(II) halides form complexes with acetonitrile and boron trihalides. The halides are bromide and chloride. These complexes form a class of their own. The mechanism of the complex formation is believed to be the halide ions transfer from the divalent metal halides to the trivalent boron halides in acetonitrile.

The nickel complexes are relatively more stable than cobalt complexes. This has been indicated by the thermal decomposition experiments of the compounds. The larger shift in the nitrile frequency in the IR spectra for Ni complexes also supports the above statement. X-ray analysis indicates these compounds are isomorphous and should have similar crystal structures. The elemental analysis and thermal analysis strongly indicates that the complexes are six-coordinated. The positive shifts of the nitrile IR frequencies upon coordination with metal ions have been interpreted as an increase in the force constant of the nitrile bond. The compounds are extremely air sensitive, they decompose rapidly when exposed to moisture in the

atmosphere. The extensive decomposition of the compounds makes spectral analyses inclusive.

After the experimental work and the analyses of the complexes were completed, the author learned that a partially related study had been carried out some ten years ago^{1a}. Some conclusions of this work are rationalized from the results of previous work.

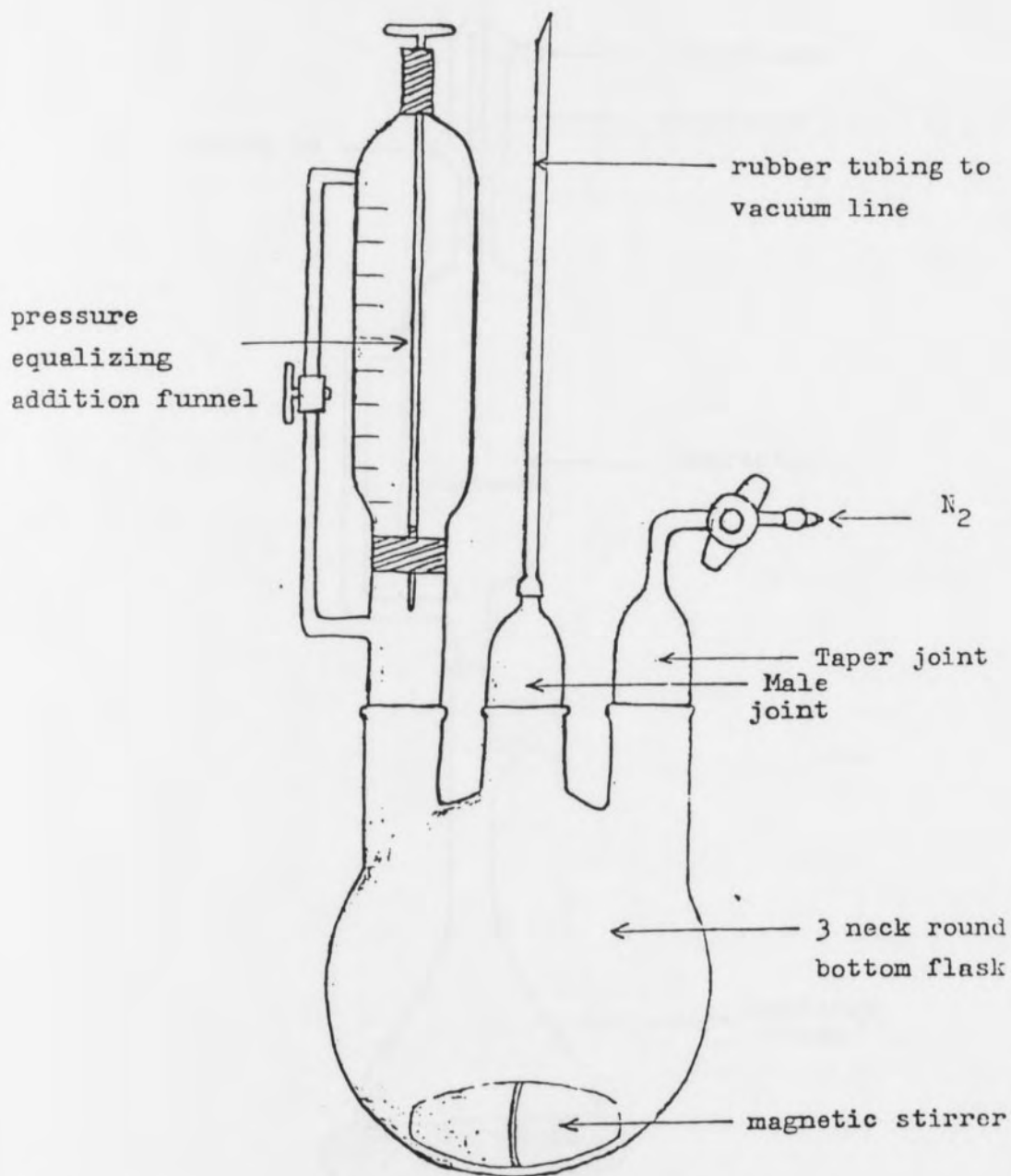


Fig.4. Apparatus for the synthesis of complexes.

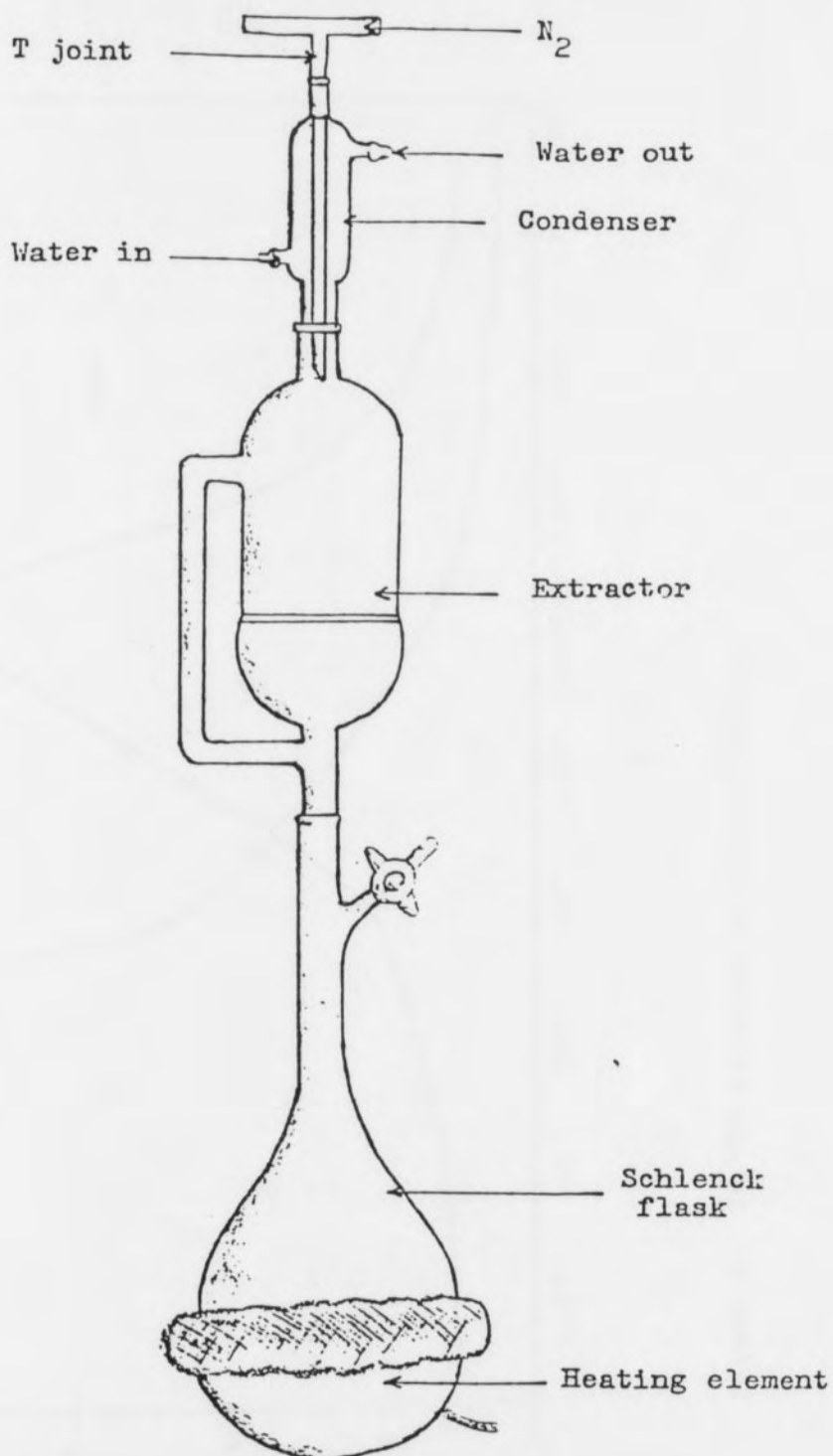


Fig 5. Extraction of the complex from impurities.

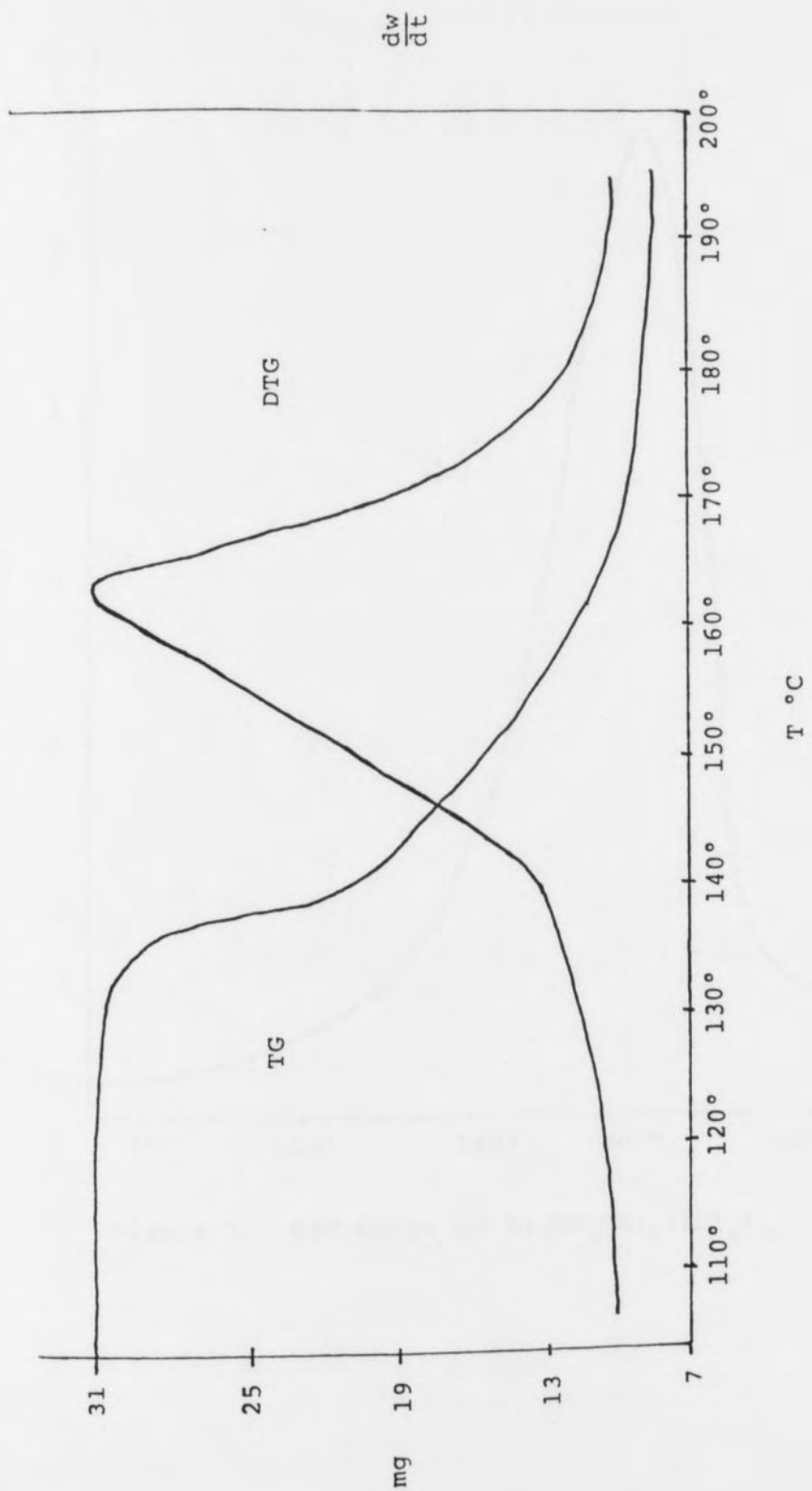


Figure 6. TG/DTG curve of $\text{Ni}(\text{CH}_3\text{CN})_6(\text{BCl}_4)_2$

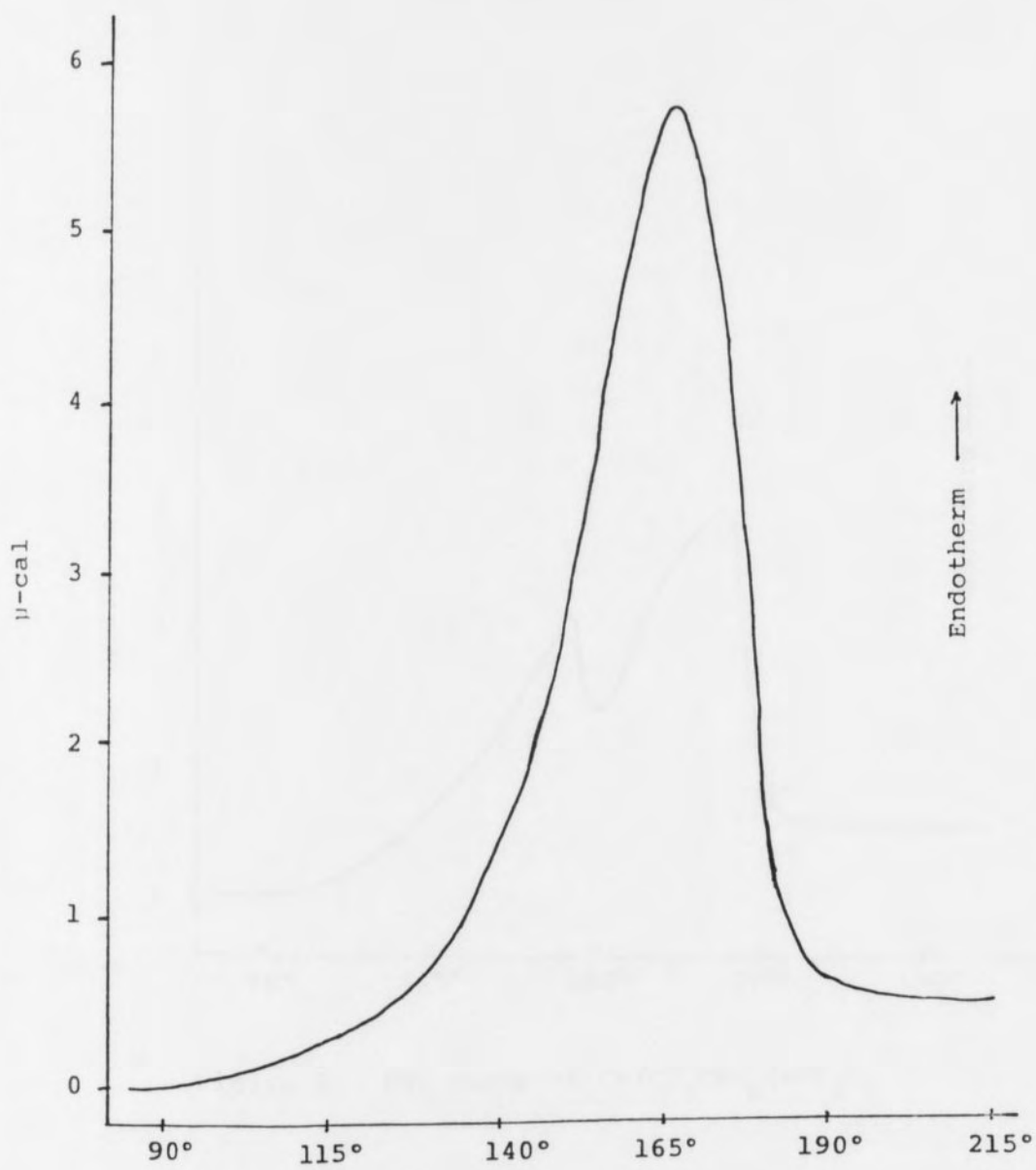


Figure 7. DSC Curve of $\text{Ni}(\text{CH}_3\text{CN})_6(\text{BCl}_4)_2$

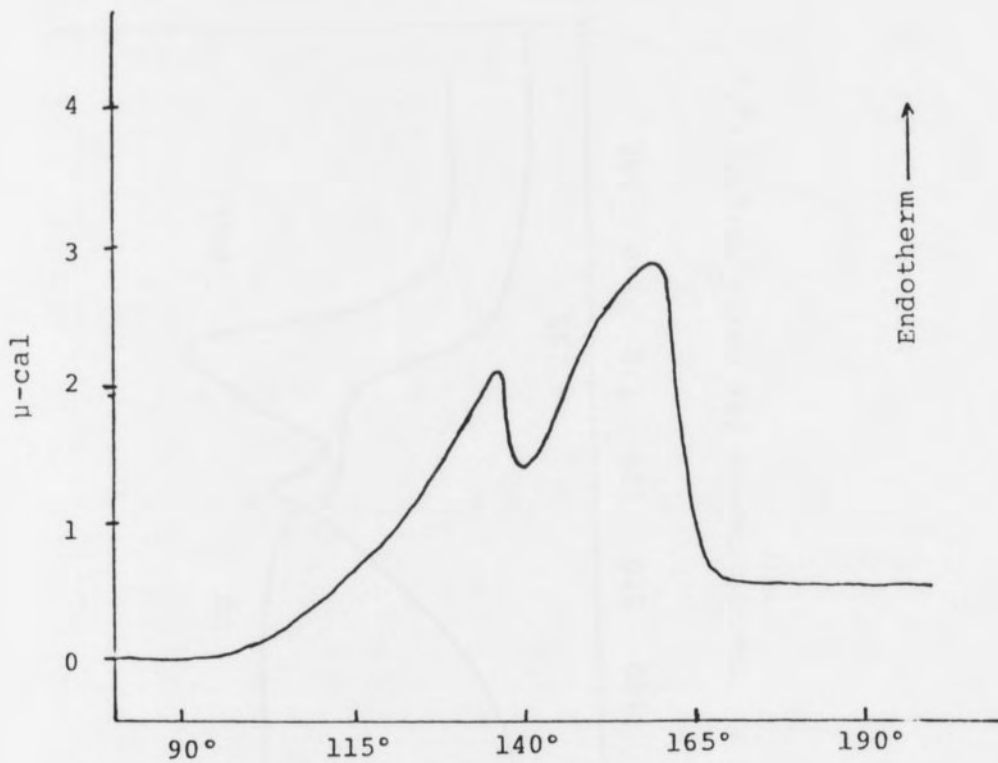


Figure 8. DSC Curve of $\text{Co}(\text{CH}_3\text{CN})_6(\text{BCl}_4)_2$

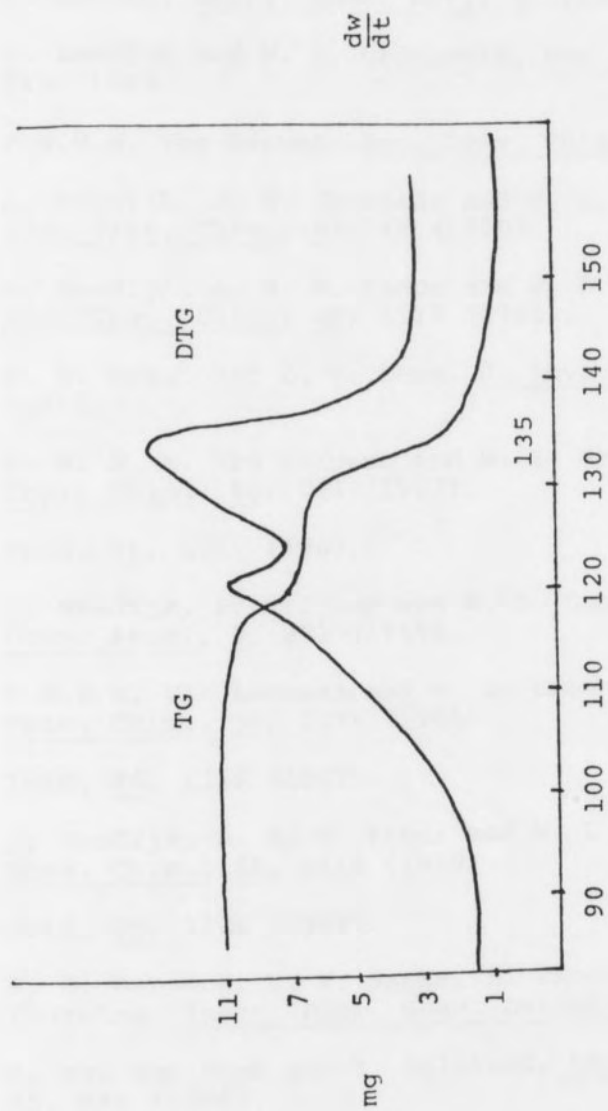


Figure 9. TG/DTG Curves for $\text{Co}(\text{CH}_3\text{CN})_6(\text{BCL}_4)_2$

BIBLIOGRAPHY

- (1) F. Basolo, Coord. Chem. Rev., 3, 213-233 (1968).
- (1a) J. Reedijk and W. L. Groenveld, Rec. Trav. Chim., 87, 513 (1968).
- (2) P.W.N.M. Van Leewen, Rec. Trav. Chim., 86, 201 (1967).
- (3) J. Reedijk, J. B. Vervelde and W. L. Groenveld, Rec. Trav. Chim., 89, 42 (1970).
- (4) J. Reedijk, A. H. M. Fleur and W. L. Groenveld, Rec. Trav. Chim., 88, 1115 (1969).
- (5) R. S. Drago and D. W. Meek, J. Phy. Chem., 65, 1146 (1961).
- (6) P. W. N. M. Van Leeuwen and W. L. Groenveld, Rec. Trav. Chim., 86, 721 (1967).
- (7) Ibid, 86, 1217 (1967).
- (8) J. Reedijk, P. Vrijhof and W. L. Groenveld, Inorg. Chim. Acta., 3, 271 (1969).
- (9) P.W.N.M. Van Leeuwen and W. L. Groenveld, Rec. Trav. Chim., 85, 1173 (1966).
- (10) Ibid, 86, 1219 (1967).
- (11) J. Reedijk, A. H. M. Fleur and W. L. Groenveld, Rec. Trav. Chim., 88, 1118 (1969).
- (12) Ibid, 88, 1124 (1969).
- (13) R. D. Hancock, H. W. Sacks, R. Thornton and D. A. Thornton, Inorg. Nucl. Chem. Letters, 3, 51 (1967).
- (14) W. Van der Veer and F. Jellinek, Rec. Trav. Chim., 85, 842 (1966).
- (15) K. F. Purcell, J. Amer. Chem. Soc., 89, 247 (1967).
- (16) J. Reedijk, A. P. Zurr and W. L. Groenveld, Rec. Trav. Chim., 86, 1127 (1967).
- (17) T. L. Brown and M. Kubota, J. Amer. Chem. Soc., 83, 4175 (1961).

- (18) A. P. Zurr, Metal Methylcyano Chloroantimonates, Thesis, Leiden 1961.
- (19) R. Schlapp and W. G. Penney, Physics Review, 41, 194 (1932).
- (20) Ibid, 42, 666 (1932).
- (21) J. Ballhausen, "Introduction to Ligand Field Theory", McGraw-Hill Book Company, Inc., New York, 58 (1962).
- (22) Ibid, 59 (1962).
- (23) Hiroshi Watanabe, "Operator Methods in Ligand Field Theory", Prentice-Hall, Inc., New Jersey, 91 (1966).
- (24) J. G. Jackson, "Classical Electrodynamics", John Wiley & Sons, Inc., New York, Chapter One (1962).
- (25) M. Gerloch and R. C. Slade, "Ligand Field Parameters", Cambridge University Press, Cambridge, Chapter Two (1973).
- (26) Ibid, Chapter Three (1973).
- (27) Ibid, Chapter Two (1973).
- (28) Hiroshi Watanabe, "Operator Methods in Ligand Field Theory", Prentice-Hall, Inc., New Jersey, Chapter Four (1966).
- (29) Condon and Shortley, "The Theory of Atomic Spectra", Cambridge University Press, Cambridge, Chapter Four (1963).
- (30) Ibid, 52 (1963).
- (31) M. Gerloch and R. C. Slade, "Ligand Field Parameters", Cambridge University Press, Cambridge, Chapter Two (1973).
- (32) J. P. Fackler, "Symmetry in Coordination Chemistry", Academic Press, New York and London, 135 (1971).
- (33) M. Gerloch and R. C. Slade, "Ligand Field Parameters", Cambridge University Press, Cambridge, 25 (1973).
- (34) J. Ballhausen, "Introduction to Ligand Field Theory", McGraw-Hill Book Company, New York, 95 (1962).
- (35) Ibid, 103 (1962).

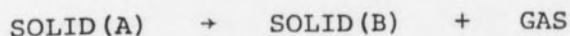
- (36) M. Gerloch, J. Lewis, G. G. Phillips and P. N. Quedsted, J.C.S., (A), 1941 (1970).
- (37) Reference (33) p. 65.
- (38) J. Reedijk, P.W.N.M. Van Leeuwen and W. L. Groenveld, Rec. Trav. Chim., 87, 140 (1968).
- (39) Horoshi Watanabe, "Operator Methods in Ligand Field Theory", Prentice-Hall, New Jersey, 149 (1966).
- (40) J. Ballhausen, "Introduction to Ligand Field Theory", McGraw-Hill Book Company, New York, 93 (1962).
- (41) A. R. Pray, Inorganic Synthesis, V, 153.
- (42) The Merck Index, 9th edition, # 2389, P. 312.
- (43) G. L. Ward, Inorganic Synthesis, XIII, 156.
- (44) Clark and Buchner, J.A.C.S., 44, 230 (1922).
- (45) Watt et al, J.A.C.S., 77, 2752 (1955).
- (46) D. T. Haworth, Inorganic Synthesis, XIV, 41.
- (47) The Merck Index, 9th edition, # 56, P. 49.
- (48) Ibid, #1362, P. 175.
- (49) G. A. Bratten, A Study of the Preparation and Characterization of Selected Complex Aluminum Hydrides, Thesis, UNC-G, 1976.
- (50) E. S. Freeman and B. Carroll, J. Phys. Chem., 62, 349 (1958).
- (51) W. K. Tang, U.S. Forest Service Research Paper, FPL 71, January, (1967).
- (52) A. W. Coates and J. P. Redfern, Nature, 201, 68 (1964).
- (53) J. Reedijk and W. L. Groenveld, Rec. Trav. Chim., 87, 521 (1968).
- (54) A. E. Wickenden and R. A. Krausa, Inorg. Chem., 4, 404 (1965).
- (55) J. Reedijk and W. L. Groenveld, Rec. Trav. Chim., 86, 1112, 1116 (1967).

APPENDIX

Equations and DSCKIN program used in thermal analyses calculations.

Equations for Thermal Analyses Calculations

Reaction:



General Equation:

$$\frac{d\alpha}{dT} = k(1-\alpha)^n$$

$$K = Ae^{-E/RT}$$

Coats-Redfern:

Zero order:

$$\log \left[-\log \frac{(1-\alpha)}{T^2} \right] = \log \frac{AR}{aE} \left[1 - \frac{2RT}{E} \right] - \frac{E}{2.3RT}$$

1/2, 1/3 and 1 order

$$\log \left[\frac{1-(1-\alpha)^{1-n}}{T^2(1-n)} \right] = \log \frac{AR}{aE} \left[1 - \frac{2RT}{E} \right] - \frac{E}{2.3RT}$$

Freeman-Carroll:

$$\frac{\Delta[\log(d\alpha/dt)]}{\Delta[\log(1-\alpha)]} = \frac{-E}{2.3RT} \left[\frac{\Delta(1/T)}{\Delta[\log(1-\alpha)]} \right] + n$$

Tang:

$$\log \left[\frac{d\alpha/dt}{(1-\alpha)} \right] = \log A - \frac{E}{2.3RT}$$

DSCIN

```
1  REM      *** DATA3 ***
2  REM      WRITTEN BY MARC WALTER      SUMMER 1976
3  REM      THIS PROGRAM CALCULATES THE HEAT OF REACTION
4  REM      AND THE ACTIVATION ENERGY FROM A DSC RUN. IT CALCULATES
5  REM      THE AREA BY SIMPSON'S INTEGRATION AND GIVES THE
6  REM      ACTIVATION ENERGY BY THREE DIFFERENT METHODS.
10 PRINT
30 LET N=0
40 DIM Y[750]
50 DIM HC[50],BC[50],KC[20]
60 DIM MC[50],SC[50],RC[50]
70 DIM Z[750]
71 DIM TC[750],QC[50]
75 LET C6=4.73637E-06
80 LET L3=1
90 PRINT "NUMBER OF MEASUREMENTS? 0 TERMINATES"
100 INPUT N
105 IF N=0 THEN 3140
110 LET J4=N
115 LET E7=0
120 PRINT "START TAPE READER"
130 PRINT
140 LET N=INT(N/10)*10
150 FOR I=1 TO N STEP 10
160 INPUT HC[1],HC[2],HC[3],HC[4],HC[5],HC[6],HC[7],HC[8],HC[9],HC[10]
170 FOR J=1 TO 10
180 LET Y[J+I-1]=HC[J]
190 NEXT J
200 NEXT I
210 REM THIS SECTION CONVERTS DATA LOGGER OUTPUT TO REAL DATA
220 PRINT "IS THIS AN EXOTHERM? 1=YES"
230 INPUT Z3
240 IF Z3=1 THEN 310
```

```

250 FOR I=1 TO N
260 IF YCII<2000 THEN 290
270 LET YCII=YCII-2000
280 GOTO 300
290 LET YCII=-YCII
300 NEXT I
305 GOTO 360
310 FOR I=1 TO N
320 IF YCII<2000 THEN 340
330 LET YCII=-(YCII-2000)
340 NEXT I
360 PRINT
370 PRINT "INPUT INITIAL TEMP,SAMPLE RATE,SCAN RATE(SEC/DEG)";
380 LET YC1]=Y[2]
390 INPUT T,R,C
400 LET C=1/C
410 REM DATA SMOOTHING FUNCTION
420 FOR I=3 TO N-2
430 LET YCII=(YCI-2]+YCI-1]+YCI]+YCI+1]+YCI+2])/5
440 NEXT I
450 REM SET UP TEMPERATURE SCALE
460 LET TC1]=T
470 FOR I=2 TO N
480 LET TCII=YCI-1]+R#C
490 NEXT I
500 REM SET UP GENERAL INDEX
503 PRINT "IS THIS A CALIBRATION RUN? 1=YES"
505 INPUT Z4
510 PRINT "INPUT THE MOLECULAR WEIGHT. INPUT 1 IF NOT KNOWN"
520 INPUT W5
530 PRINT "RANGE IN MCAL/SEC";
540 PRINT
550 INPUT R2
560 LET K6=1
570 LET K7=(R/1)*(R2/8)*K6

```

```

580 REM THIS CONVERTS DATA LOGGER INPUT TO MM
590 FOR I=1 TO N
600 LET Y[I]=Y[I]*.255
610 NEXT I
620 PRINT "INPUT SAMPLE WEIGHT IN MG";
630 INPUT W7
640 LET W7=W7/1000
650 REM THIS SETS PARAMETERS FOR FINDING THE PEAK START
660 LET Y5=3
670 LET K1=1
680 LET K2=10
690 LET K4=N-5
700 LET K5=1
710 LET L=1
720 LET K3=1
730 REM JUMP TO PEAK FINDING ROUTINE
740 GOSUB 1110
750 REM SET UP TO FIND END OF PEAK
760 LET P5=S
770 REM SAVE SLOPE AND INTERCEPT FOR BASELINE CORRECTION
780 LET B5=B
790 LET M5=M
800 LET K3=-1
810 LET K1=N
820 LET K4=N-K4
830 GOSUB 1110
840 LET B4=B
850 LET M4=M
860 LET B=S
870 LET S=P5
880 PRINT
890 PRINT
900 PRINT "PEAK STARTS AT";T[C5];"DEGREES AND ENDS AT";T[C6];"DEGREES"
910 GOSUB 1530
920 PRINT "DO YOU WANT TO CHANGE THE START,MIDDLE OR END OF THE PEAK?"

```

```
930 PRINT "FOR INTEGRATION? 1=YES"  
940 INPUT Z  
950 IF Z <> 1 THEN 1100  
960 PRINT "INPUT THE START OF THE PEAK IN DEGREES"  
970 INPUT Z1  
980 PRINT "INPUT THE MAXIMUM "  
990 INPUT Z3  
1000 PRINT "INPUT THE END OF THE PEAK"  
1003 INPUT Z2  
1005 FOR I=1 TO N  
1006 IF T(I)>Z3 THEN 1012  
1009 LET F6=1  
1012 IF T(I)>Z1 THEN 1018  
1015 LET S=I  
1018 IF T(I)>Z2 THEN 1023  
1020 LET B=I  
1023 NEXT I  
1025 GOSUB 1085  
1027 IF E3 <> 1 THEN 3150  
1030 LET E5=S  
1033 LET E6=B  
1036 LET K1=1  
1039 LET K3=1  
1040 LET E7=10  
1043 LET K2=S  
1046 LET K4=N-5  
1048 GOSUB 1110  
1050 LET B5=B  
1053 LET M5=M  
1056 LET K1=N  
1058 LET K3=-1  
1060 LET K2=N-E6  
1063 LET K4=N-K4  
1066 GOSUB 1110
```



```

1068 LET B4=B
1070 LET M4=M
1073 LET S=E5
1076 LET B=E6
1080 GOTO 1670
1085 PRINT "FOR SLOPE CALCULATED BASELINE ENTER 1, 0 GIVES"
1087 PRINT "2 POINT LINE METHOD."
1089 INPUT E3
1090 RETURN
1100 GOTO 1670
1110 REM : THIS ROUTINE FINDS THEN BEGINNING OR END OF A
1120 REM : PEAK.
1130 LET G=1
1140 LET L5=L/2
1150 LET K8=K5-L
1160 LET K9=K3*(K4-K1)
1170 LET T=0
1180 LET T2=0
1190 LET W=0
1200 LET P=0
1210 LET W2=0
1220 LET S=K1-K3
1230 LET N3=0
1240 REM CALCULATE LEAST SQUARES UP TO N3
1250 LET S=S+K3
1260 LET N3=N3+1
1270 LET T=T+S
1280 LET T2=T2+S^2
1290 LET W=W+Y[S]
1300 LET P=P+S*Y[S]
1310 IF N3<K2 THEN 1250
1313 IF E7 <> 10 THEN 1320
1315 GOTO 1330
1320 IF N3>K9 THEN 1510
1330 LET M=(N3*P-T*W)/(N3*T2-T^2)

```

```

1340 LET B=(W*T2-T*P)/(N3*T2-TT2)
1345 IF E7 <> 10 THEN 1350
1347 RETURN
1350 REM TEST FOR DEVIATION FROM CALCULATED LINE
1360 FOR J=1 TO 3
1370 LET JB=S+K3*(K8+J*L)
1380 LET Y4=0
1390 FOR I=JB-1 TO JB+1
1400 LET Y4=Y4+Y[C I]
1410 NEXT I
1420 LET Y4=Y4/3
1430 LET DB=Y4-B-M*JB
1440 IF ABS(DB)<Y5 THEN 1250
1450 NEXT J
1460 LET H6=B+M*S
1470 GOTO 1500
1480 LET S=K4
1490 LET G=0
1500 RETURN
1510 PRINT "PEAK NOT SENSED"
1520 STOP
1530 REM **LOOK FOR PEAK MAXIMUM,P6
1540 LET D=0
1550 LET P6=0
1560 FOR I=S+2 TO B
1570 FOR J=1 TO 6
1580 LET D=Y[C I+J]-Y[C I+J+1]
1590 IF D<0 THEN 1620
1600 NEXT J
1610 GOTO 1630
1620 NEXT I
1630 PRINT "PEAK MAX AT";T[C I];"DEGREES";I;"INDEX"
1640 PRINT
1650 LET P6=I
1660 RETURN

```

```

1670 REM **CORRECT Y(I)VALUES FOR BASE LINE DRIFT AND ZERO
1680 GOSUB 2520
1690 GOSUB 1710
1700 GOTO 1880
1710 REM **INTEGRATION ROUTINE USING SIMPSON'S METHOD
1720 LET L3=1
1730 LET R6=1/3
1740 LET A2=0
1750 LET A4=Y[S+1]
1760 LET Y7=Y[S]
1770 LET S5=S+2
1780 LET S6=B-2
1790 REM SUMATION ROUTINE
1800 FOR I=S5 TO S6 STEP 2
1810 LET A2=A2+Y[I]
1820 LET A4=A4+Y[I+1]
1830 REM GO TO GET PARTIAL AREAS
1840 GOSUB 1990
1850 NEXT I
1860 LET P5=R6*(Y7+2*A2+4*A4+Y[S6])
1870 RETURN
1880 PRINT
1890 PRINT "AREA";
1892 PRINT "  ";P5
1895 IF Z4 < 1 THEN 1900
1896 REM THE MAIN INTEGRATION.
1897 LET C6=.779492*W7*1000/(W5*P5*R*R2)
1898 GOTO 3300
1900 LET C9=C6*P5*R*R2
1910 LET F2=(C9*W5)/(W7*1000)
1920 IF W5=1 THEN 1950
1930 PRINT "HEAT OF REACTION =" ;F2; "KCAL/MOLE"
1940 GOTO 1970
1950 PRINT "HEAT OF REACTION =" ;F2; "KCAL/GRAM"
1970 PRINT

```

```

1980 GOTO 2060
1985 REM PARTIAL AREA INTEGRATION BY STRIPPING OFF VALUES FROM
1990 IF I<((B-S)/B)*L3+S THEN 2050
2000 IF I>B-2 THEN 2050
2005 REM Q( ) =PARTIAL AREA M( )= HEIGHT AT I
2010 LET QCL3]=R6*(Y7+2*A2+4*A4+Y[C I+2])
2020 LET MCL3]=Y[C I+2]
2030 LET ZCL3]=I+2
2040 LET L3=L3+1
2050 RETURN
2060 PRINT 'DO YOU WANT KINETICS? 1=YES'
2070 INPUT Z
2080 IF Z <> 1 THEN 3130
2090 GOTO 2160
2100 LET T=0
2110 LET T2=0
2120 LET W=0
2130 LET F=0
2140 LET W2=0
2150 RETURN
2160 FOR I=2 TO L3-2
2170 GOSUB 2100
2180 REM GET SLOPE OF LINE AT Z(I) FOR KINETICS
2190 FOR J=Z[C I]-2 TO Z[C I]+2
2200 LET T=T+J
2210 LET T2=T2+J^2
2220 LET W=W+Y[C J]
2230 LET F=F+J*Y[C J]
2240 NEXT J
2250 LET M=(5*F-T*W)/(5*T2-T^2)
2260 LET T5=T[Z[C I]]+273
2270 REM CALCULATE TWO VARIABLES
2280 LET S[C I]=(1-(Q[C I]/P5))/(M[C I]*T5^2)
2290 LET R[C I]=(1-(Q[C I]/P5))*M/M[C I]^2
2300 LET B[C I]=M

```

```

2310 NEXT I
2320 LET C8=C
2330 GOSUB 2100
2340 REM PLOT THE TWO CALCULATED PARAMETERS
2350 FOR I=2 TO L3-2
2360 LET W2=W2+RCIJ^2
2370 LET T=T+SCIJ
2380 LET T2=T2+SCIJ^2
2390 LET W=W+RCIJ
2400 LET P=P+SCIJ*RCIJ
2410 NEXT I
2420 LET M=((L3-3)*P-T*W)/((L3-3)*T2-T^2)
2430 LET B7=(W*T2-T*P)/((L3-3)*T2-T^2)
2440 LET E=M*1.9872/(C*1000)
2450 LET N=-B7*P5
2460 PRINT "THE ACTIVATION ENERGY =";E;"KCAL/MOLE"
2470 PRINT "THE ORDER OF THE REACTION IS ";N
2480 GOSUB 3100
2490 PRINT "THE CORRELATION COEFFICIENT =";C
2500 PRINT
2510 GOTO 2610
2520 REM BASELINE CORRECTION USING LEAST-SQUARES FROM EACH SIDE
2530 REM TO THE CENTER OF THE PEAK
2540 FOR I=1 TO P6
2550 LET YC[I]=Y[C[I]]-(B5+M5*I)
2560 NEXT I
2570 FOR I=P6+1 TO N
2580 LET YC[I]=Y[C[I]]-(B4+M4*I)
2590 NEXT I
2600 RETURN
2610 PRINT "DO YOU WANT TO CONTROL THE ORDER? 1=YES"
2620 INPUT I
2630 IF I <> 1 THEN 2880
2640 PRINT "INPUT THE ORDER. NEGATIVE NUMBER TERMINATES"

```

```

2650 INPUT N
2660 IF N<0 THEN 2880
2670 LET S3=0
2680 LET S1=0
2690 PRINT " TEMPERATURE      ACTIVATION ENERGY"
2700 FOR I=2 TO L3-2
2710 LET T5=T[Z[I]]+273
2720 LET E=1.9872*T5^2*(B[I]+(N*M[I]^2/((1-Q[I]/P5)*P5)))
2730 LET E=E/(M[I]*1000*CB)
2740 LET S3=S3+E
2750 LET H[I]=E
2760 PRINT T[Z[I]],E
2770 NEXT I
2780 LET S2=S3/(L3-3)
2790 FOR I=2 TO L3-2
2800 LET S1=S1+(H[I]-S2)^2
2810 NEXT I
2820 LET S1=SQR(S1/(L3-5))
2830 LET S0=1-S1/S2
2840 PRINT "THE AVERAGE ACTIVATION ENERGY IS";S2;"KCAL/MOLE"
2850 PRINT "THE STANDARD DEVIATION IS ";S1
2860 PRINT
2870 GOTO 2640
2880 GOSUB 2100
2885 REM CONVERT Y(I) TO MCAL/SEC
2890 FOR I=1 TO J4
2900 LET Y[I]=Y[I]*.004*R2/8
2910 NEXT I
2915 REM GET AREAS FOR NEW Y(I) VALUES
2920 GOSUB 1710
2930 FOR I=2 TO L3-2
2940 LET K[I]=M[I]/(P5-Q[I])
2950 LET T5=(1/(T[Z[I]]+273))*1000
2960 LET T=T+T5
2970 LET T2=T2+T5^2

```

```

2980 LET W=W+LOG(KCII)/2.303
2990 LET W2=W2+(LOG(KCII)/2.303)^2
3000 LET F=F+(LOG(KCII)/2.303)*T5
3010 NEXT I
3020 LET E=((L3-3)*F-T*W)/((L3-3)*T2-T^2)
3030 LET E=-E*2.303*1.9872
3040 PRINT "ASSUMING THAT THE ORDER IS ONE, THE ACTIVATION"
3050 PRINT "ENERGY IS";E;"KCAL/MOLE"
3060 GOSUB 3100
3070 LET C=-C
3080 PRINT "THE CORRELATION COEFFICIENT =" ;C
3090 GOTO 3130
3095 REM CALCULATE CORRELATION COEFFICIENT FROM LEAST
3096 REM SQUARES DATA.
3100 LET C=((L3-3)*F-T*W)
3110 LET C=C/SQR(((L3-3)*T2-T^2)*((L3-3)*W2-W^2))
3120 RETURN
3130 GOTO 80
3140 GOTO 3270
3150 LET M=(Y[B]-Y[S])/(B-S)
3160 LET V2=Y[S]-M*S
3230 FOR I=1 TO N
3240 LET YCII=YCII-(V2+M*I)
3250 NEXT I
3260 GOTO 1690
3270 GOTO 4000
3300 PRINT "CHANGE C6 IN LINE 75 TO " ;C6
3310 GOTO 4000
4000 END

```